Application of Fiber Amplifiers

to

Fiber Lasers and Terahertz Spectroscopy

Thesis by

Namkyoo Park

In Partial Fulfillment of the Requirements

for the Degree of

Doctor of Philosophy

California Institute of Technology

Pasadena, California

1994

(Submitted April 26, 1994)

To my parents

with all of my love

Acknowledgments

Five years ago, when I started studying for my degree, my roommate told me that the most important character one needs to finish a Ph.D. degree is patience. Also, I remember Pete's acknowledgement in which he compared a Ph.D. to a marathon. Now I can agree.

The last five years of my study was a path towards the new world of science, as well as a period during which I have learned more about myself. For the most of the time, it was my advisor Dr. Kerry Vahala who encouraged me to stay in the direct path toward the goal. I appreciate his guidance which made it possible for me to finish my degree successfully with both broad experience in my chosen field and with many interesting results.

Part of this work involved productive collaborations with other members of our group. For this, I give special thanks to Dr. Jay Dawson, Jianhui Zhou, and Dr. Steve Sanders. My work with them was full of fun and successful results. It was also fun to talk with Pete about various problems in the life and science. John was kind, and I still appreciate his work on digitizing my face into the good old MacII. Mike, Charles, Robert and Dave are good friends and I appreciate the times we have had together. I would like to thank Rosalie Rowe for her help with day to day matters.

My times with Korean students in Caltech were also great, even though our activity was mostly limited to movies and beers. I want to express special thanks to Jayhyoung, Wooyoung and Geunchang, as well as Junhyeong. I would also like to thank Johan for his patience in correcting all the mistakenly placed "a"s and "the"s

in my thesis manuscript. As this thesis was dedicated to my parents, I think it would have been impossible for me to overcome emotional difficulties without the support and prayers of my parents, my brother and my sister. I will always love them.

Abstract

Starting with a review of the Erbium doped fiber amplifier, this thesis will describe the construction, intensity noise, linewidth, stabilization techniques, and spectroscopic applications of the Erbium doped fiber ring laser developed as a part of the thesis research activity. This laser, which uses the Erbium doped fiber amplifier as its gain module within fiber based ring resonator, exhibits excellent sidemode suppression (>70dB) and intensity noise properties (shot noise limited beyond GHz regime) with ultranarrow linewidth (<4kHz).

To measure and improve these performance, several new techniques were developed. : A new interferometer based on a loss-compensated recirculating delayed self heterodyne technique, for the measurement of ultranarrow linewidth. A novel intracavity filtering technique to make the laser operate at the shot noise floor of intensity noise. Extension of Pound-Drever locking technique into the laser cavity, to enable the laser be stabilized and locked to an external reference at the same time.

The laser was also applied as a spectroscopic tool to study the four wave mixing process in semiconductor optical amplifiers. Because of the ultranarrow linewidth and intensity noise characteristics of fiber laser, it was possible to resolve THz intraband dynamics in a quantum well amplifier.

This thesis will also cover mode locked operation of the fiber laser and related issues briefly in the appendix.

Contents

1 Introduction **1**

1.1 Fiber lasers 1

1.2 Outline of thesis 2

2 Erbium Doped Fiber Amplifiers **6**

2.1 Background 6

2.2 Optical fiber amplifiers 8

2.3 Characterization of an EDFA 11

3 Fiber Lasers **22**

3.1 Single mode fiber lasers 22

3.2 Erbium doped fiber ring lasers (EDFRL) 24

4 Noise Characteristics of the EDFRL **35**

4.1 Intensity noise 36

4.1.1 Theory 36

4.1.2 Balanced homodyne detection 40

4.1.3 Measurement 41

4.2 Frequency noise 47

4.2.1 Theory 47

4.2.2 Recirculating DSHI 48

4.2.3 Measurement 56

5 Frequency Locking of an EDFRL to an External Cavity **62**

5.1 Pound-Drever method 62

5.2 Implementation of the locking technique to the fiber laser 65

6 Application of EDFRL to Four-Wave Mixing **71**

6.1 FWM in the traveling wave amplifier 72

6.2 Application of EDFRL to the FWM experiment 75

6.3 Wavelength Conversion with FWM 78

A Mode Locked Operation of Fiber Lasers **84**

A.1 Nonlinearities in fiber 84

A.2 Mode locked fiber laser 86

List of Figures

2.1 Typical cross-sectional structure of an Erbium doped fiber 9

2.2 Standard structure of an EDFA 10

2.3 Impact of EDFA on optical communication 12

2.4 Set up for EDFA characterization 16

2.5 Typical gain curve of an EDFA 17

2.6 EDFA gain as a function of pump power 18

3.1 Spatial hole burning effect 25

3.2 Schematic of an Erbium doped fiber ring laser 27

3.3 Erbium doped fiber ring laser output power 28

3.4 Erbium doped fiber ring laser lasing spectrum 29

3.5 Erbium doped fiber ring laser tuning curve 31

3.6 Parameters involved with sidemode suppression 32

4.1 Relaxation oscillation frequency of a single mode laser 37

4.2 Relative intensity noise of a single mode laser 38

4.3 Spectrum of the beating noise from an EDFRL 39

4.4 Balanced homodyne detection system 40

4.5 Measured EDFRL intensity noise 43

4.6 Spectral filtering for minimum noise operation 44

4.7 Calculated intensity noise with spectral filtering concept 45

4.8 Measured intensity noise with spectral filtering concept 46

4.9 Conceptual drawing for the frequency noise behavior 48

4.10 Self heterodyne interferometer for linewidth measurement 49

4.11 Structure of a recirculating delayed self heterodyne interferometer . . 51

4.12 Output spectrum from the RDSHI 53

4.13 EDFA effect on laser linewidth 54

4.14 EDFA effect on RDSHI S/N ratio 55

4.15 High resolution spectrum of the RDSHI output 58

4.16 Measured linewidth vs. delay-line length 59

5.1 Pound-Drever concept 63

5.2 Feedback diagram for laser stabilization 66

5.3 Error signals from the feedback circuitry 69

6.1 Intraband dynamics involved with the FWM process 73

6.2 FWM process in TWA 74

6.3 Measurement setup for FWM experiment 77

6.4 Measured FWM signal as a function of detuning frequency 79

6.5 Required TWA gain for lossless wavelength conversion 81

A.1 Pulse propagation in a dispersive, nonlinear medium 87

A.2 Schematic of a passively mode locked laser 89

A.3 Soliton pulse compression 90

A.4 Output from a mode locked fiber laser 91

Chapter 1

Introduction

1.1 Fiber lasers

Good laser sources at 1.5μm have special importance when compared to equivalent lasers at other frequency ranges. The lowest loss (0.15dB/km) of the optical fiber at this wavelength, wih the Erbium doped fiber amplifier (EDFA) make this frequency range to be one of the most promising windows for optical communication. Lasers at this wavelength can therefore be useful as a source or as a characterization tool for other devices.

With the rapid development of Erbium doped fiber amplifier (EDFA), and the interest in the sources which are compatible with the EDFA, research on fiber lasers has been very active for past several years. For example, the fiber grating based single frequency laser, even with its limited tuning capability, has demonstrated its potential usefulness in WDM systems [3]. The actively mode-locked fiber laser demonstrated the error free generation of picosecond solitons at 20GHz repetition rate [1, 2]. The

single-frequency tunable fiber ring laser, developed in Caltech, which will be described in this thesis, has demonstrated large sidemode suppression, ultra-narrow linewidth, large tuning range and excellent noise properties [5, 6, 7, 8]. The single frequency ring laser has also been successfully applied for the study of femtosecond dynamics in semiconductor optical amplifiers [4, 9].

1.2 Outline of thesis

In this thesis, the basic concept, construction and noise characteristics of an Erbium doped fiber ring laser will be described, from both experimental and theoretical viewpoints. The physics of the Erbium-doped fiber amplifier and the application of the Erbium fiber ring laser to Terahertz spectroscopy will be included as independent chapters of discussion. A laser stabilization and locking technique will also be described.

Chapter 2 will present an overview of the Erbium-doped fiber amplifier. The impact of the EDFA in optical communication systems will be described, along with brief descriptions about the latest developments in fiber-optic devices. A detailed theoretical model for the EDFA will be presented along with experimental techniques for characterizing EDFA performances.

In chapter 3 the concept of the tunable, single longitudinal-mode fiber laser will be described. First, different approaches for the single-mode operation will be assessed, with discussions on the difficulties encountered in realizing fiber-based single-mode tunable lasers. The relation between the unidirectional ring resonator geometry and

the spatial hole burning problem will be then explained, along with the tandem fiber Fabry-Perot filter concept which was applied here for stable, widely tunable operation of the laser. The laser performance characteristics such as tuning range, output power, and sidemode suppression will be summarized at the end.

Chapter 4 will be dedicated to the discussion for the noise characteristics of the fiber laser. The first half of the chapter will describe the intensity noise characteristics of the laser in various frequency domains. The intensity noise theory, measurement technique will be explained with the calibrated noise measurement relative to the shot noise level. Noise reduction techniques with intracavity spectral filtering concept will be demonstrated. The latter half of chapter 4 will also include a discussion about the phase and frequency noise of the laser. The linewidth and frequency jitter of the laser will be analyzed with a high resolution recirculating delayed self heterodyne interferometer (RDSHI) which has been developed for the sub-kHz linewidth measurement. The principle of the operation of the RDSHI will also be explained.

Chapter 5 will describe application of the Pound-Drever locking technique to fiber laser. An extension of the technique, inside the laser cavity, will be demonstrated in fully fiber optic version, to achieve locking the EDFRL to an external fiber Fabry-Perot cavity and at the same time to stabilize the laser against mode hopping.

Chapter 6 will describe application of the EDFRL to semiconductor optical traveling-wave amplifier (SOA) Terahertz spectroscopy, through four-wave mixing (FWM) process. The advantages of the fiber laser for this application will be explained. Brief discussion about the dynamics involved in the four-wave mixing process in SOA will

be given, along with the theory and measurement. The possibility of using the SOA FWM as a wavelength conversion device will be investigated by estimating the FWM conversion efficiency of the device.

The appendix will include a brief discussion of mode locked operation of fiber lasers, along with a related study about nonlinearities in the fiber, and numerical simulations of soliton propagation inside the fiber.

Bibliography

[1] H. Takara, S. Kawanishi, and M. Saruwatari, Electron. Lett. **29**, 1149 (1993)

[2] A. D. Ellis, T. Widdowson, X. Shan, G. E. Wickens, and D. M. Spirit, Electron. Lett. **29**, 990 (1993)

[3] A. D. Kersey, T. A. Berkoff, and W. W. Morey, Electron. Lett. **28**, 236 (1993)

[4] J. Zhou, N. Park, J. Dawson, K. Vahala, M. Newkirk, and B. Miller, Appl. Phys. Lett., **63**, 1179, (1993)

[5] N. Park, J. Dawson, K. Vahala and C. Miller, Appl. Phys. Lett., **59**, 2369, (1991)

[6] N. Park, S. Sanders, J. Dawson, and K. Vahala, Proc. Conf. Lasers and Electro-Otics, **CLEO 92**, (1992), paper CWE5

[7] S. Sanders, N. Park, J. Dawson, and K. Vahala, Appl. Phys. Lett., **61**, 1889, (1992)

[8] N. Park, J. Dawson, and K. Vahala, Opt. Lett., **17**, 1274, (1992)

[9] J. Zhou, N. Park, J. Dawson, K. Vahala, M. Newkirk, and B. Miller, Photon. Tech. Lett., **6**, 50, (1994)

Chapter 2

Erbium Doped Fiber Amplifiers

The Erbium doped fiber amplifier, which constitutes the gain element of the Erbium doped fiber ring laser, will be discussed in this chapter. The importance of the EDFA in optical communication systems will be described, and a theoretical analysis will be presented to better understand the physics of its operation.

2.1 Background

Before studying the physics and characteristics of Erbium doped fiber amplifier (EDFA), it will be helpful to review some of the passive and active devices used in optical communication. Components include fused fiber couplers, splitters, wavelength division multiplexers (WDM), fiberoptic isolators, and recently developed fiber gratings. Some of these components had been developed before the emergence of EDFA, but other components have gained in importance only by needs which have been generated by EDFA. In general, most of the bulk optic components now have a fiberoptic

counterpart which can be purchased off the shelf. Active devices like acousto-optic modulators, electro-optic modulators, laser diodes are also common stock items with nominal pigtailing costs. Pigtailing of these components decreases the connection loss and backreflection between components in fiber optic links.

Integration of components into the fiber itself is also very popular. These devices include magnetic material codoped fibers for fiber isolators, polarizing fibers [9], fiber loop mirrors [10], fiber Fabry-Perots [11], fiber gratings [12], fiber optic modulators [13] and higher Kerr fibers [14].

The EDFA has emerged as a natural part of this trend, but the performance of EDFA has greatly surpassed all expectations. Much of the reason for this is related to the fiber environment itself. For example, the energy splitting due to the stark effect in the fiber glass host expands the available gain bandwidths of EDFA. The excellent overlap between the pump and the signal beam inside the waveguiding structure of fiber makes the energy transfer from pump to signal almost perfect, yielding small signal gains as high as 40dB. Power optimized EDFAs can deliver output power as high as 27dBm [16]. The noise figure of the EDFA also can be made as low as 3dB under conditions of complete inversion of ions inside the fiber core (with 980nm pumping).

The almost perfect branching ratio of Erbium ions from the pumped state to the upper level of the transition is the other key factor in making these high efficiencies possible. Together with the reduced channel crosstalk from the long spontaneous lifetime ($\sim$12ms) of the Erbium ion [15] and the available wide gain bandwidth, it

makes multiple channel operation of EDFA easier than with other types of optical amplifiers.

2.2 Optical fiber amplifiers

Even though the 3rd communication window at 1.5 μm provides the lowest loss and wide bandwidth, there still exists unavoidable attenuation in the fiber from the material itself. To compensate this problem of signal attenuation, optical amplifiers (Raman amplifier, Brioullin amplifier or semiconductor optical amplifier) [1, 2, 3] or signal regenerators had to be used at every tens of km fiber lengths. Still, these devices have had limited capabilities from low efficiencies, limited bandwidth [1, 2], channel crosstalk, or data format dependencies [4].

Less than 10 years ago scientists at the University of Southampton revisited the topic of all optical amplification inside an optical fiber by studying rare-earth doping of the fiber core [5]. Surprisingly, it took only a few years of added focused research by the communication industry to realize a commercial grade single mode fiber optical amplifier, using the rare earth Erbium as an added core dopant (figure 2.1). With the EDFA, it was possible to resolve many of the problems existed before for other types of amplifiers.

Figure 2.2 shows the basic structure of an EDFA, along with the simplified energy band diagram of an Erbium ion inside a glass host. Usually, a temperature controlled, pigtailed laser diode at 980nm or 1480 nm is used as the pump source. Pumping at other wavelengths is also possible, but produces much lower pumping efficiencies [17].

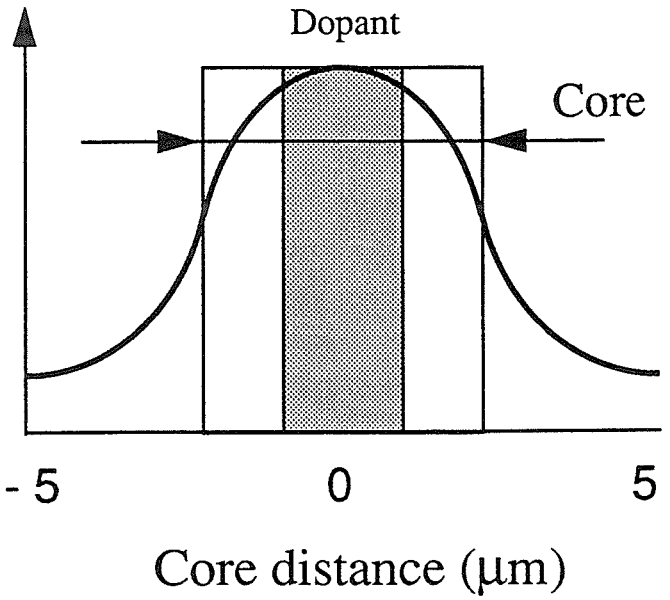

Figure 2.1: Typical structure of rare earth doped fiber. The dopant is usually concentrated at the center of the fiber core where it encounters higher pump beam intensity.

The output of the pump laser is coupled to the Erbium doped fiber through a fused fiber wavelength division multiplexer. These elements can be put together by using either connectors or splices. Leaking pump power from the open port of a WDM can be used to feedback and stabilize the pump source. The input signal couples to the EDF through the WDM, and experiences amplification as it propagates through the inverted gain medium. Since the gain of the EDFA is very high, minute reflections from the facets of the cleaved fiber can give rise to oscillation. To suppress the possible oscillation of an EDFA, optical isolators are usually placed at the ends of the EDFA unit.

It is also possible to make variations on this basic configuration. Placing an extra

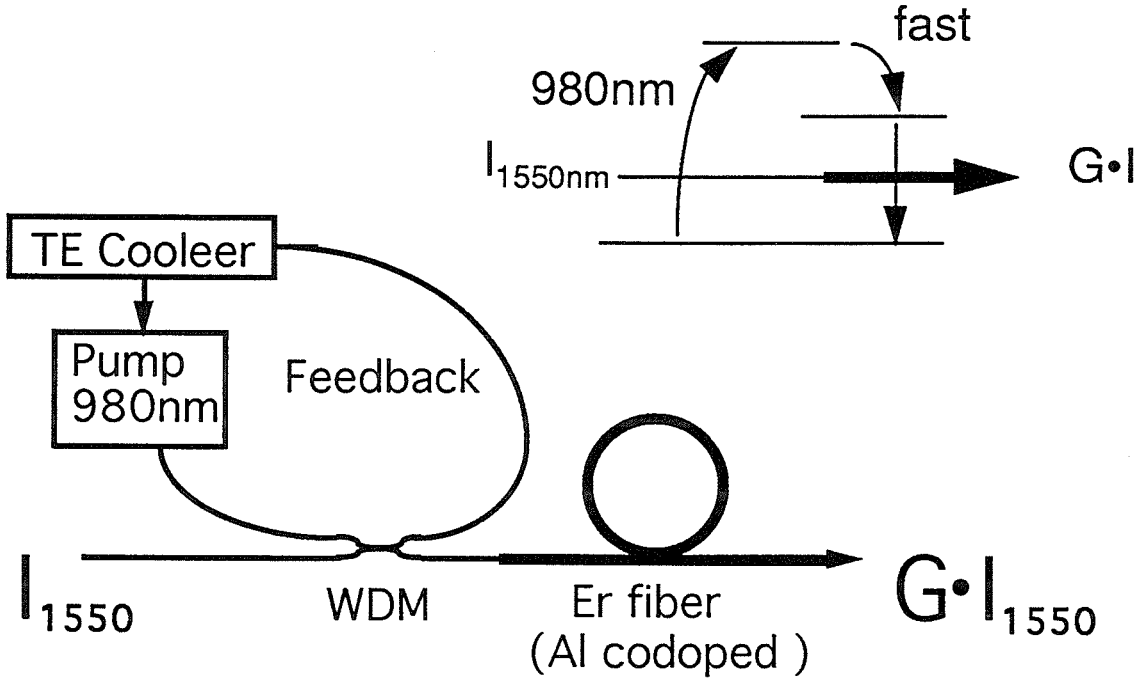

Figure 2.2: Schematic diagram of an EDFA. The optical beam experiences amplification from stimulated emission as it propagates through the inverted gain medium.

isolator in the middle of an EDFA can reduce the backward propagating ASE which eats up the gain and increases the noise figure of an EDFA. Bi-directional pumping and counter directional pumping are also useful for specific applications [23].

With this simple structure, EDFA features high single pass gain, high saturation output power with low signal crosstalk, quantum limited noise, and negligible polarization dependence [7, 8]. In addition it can be pumped efficiently at 1480μm and 980μm, both bands that are attainable using commercially available semiconductor lasers [6].

With all of these attributes, EDFA have quickly become a key component in long-haul telecommunication systems. Indeed, the impact of EDFAs in the optical communication industry has been quite dramatic (figure 2.3). It has also been chosen for the use in the 5 Gb/s link between the U.S. and Japan which is scheduled for installation in 1995. Low crosstalk between channels combined with the wide gain bandwidth of EDFA might ultimately result in their use in future wavelength division multiplexing based systems [8]. They might also have a roll in future local area networks.

2.3 Characterization of an EDFA

To describe the performance of an EDFA, one needs to specify its gain, saturation output power and noise figure. These quantities depend on several parameters such as input signal level and wavelength, pumping direction, pump power and pump wavelength, as well as the characteristics of fiber (length, doping profile and concentration,

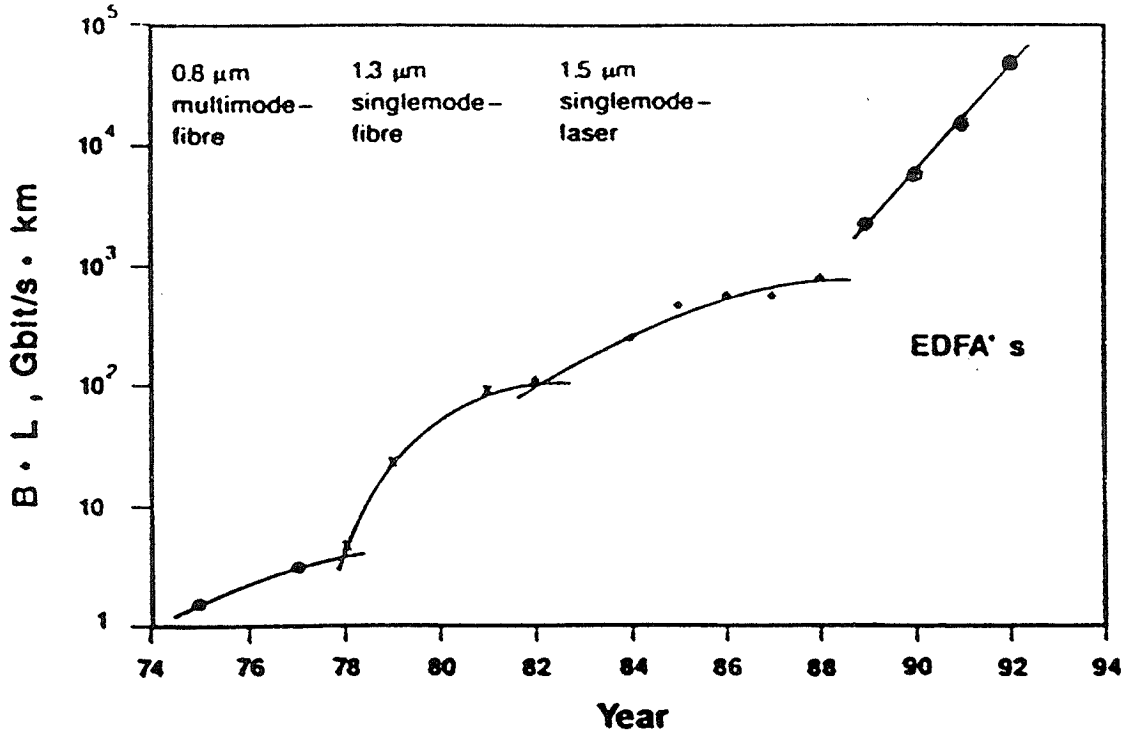

Figure 2.3: The graph shows the change in slope for the bit rate - span length product after the introduction of EDFA.

and the structure of the fiber) [18]. All of these characteristics and parameters can be measured experimentally [19, 20].

Still, when one needs to understand or to predict the behavior of the EDFA with a relatively small set of data, it is necessary to rely on theoretical models based on rate equations. The most accurate solution to these rate equations can only be obtained from numerical analysis, since most analytic approaches oversimplify the effect of amplified spontaneous emission and tend to fail at gain levels higher than 20dB [18]. In addition, with the numerical approach, it is not only possible to treat the presence of multiple signals and ASE precisely, but also to predict the performance of an EDFA based on its structure [18].

The most common approach takes spatial-aaveraging technique. By spatially averaging input parameters like the beam shape, doping and index profiles inside the fiber, the equations for EDFA can be characterized in terms of a few sets of parameters such as gain or absorption per unit length and saturation power. These equations then can be easily solved with the standard Runge-Kutta method [21].

If one writes the power $P_k(z)$ of an optical beam (pump or signal) at wavelength λ_k and the normalized intensity $i_k(r,\phi)$ of the beam inside the fiber as follows,

$$P_k(z) = \int_0^{2\pi}\int_0^{\infty} I_k(r,\phi,z)\, r dr d\phi \tag{2.1}$$

$$i_k(r,\phi) = \frac{I_k(r,\phi,z)}{P_k(z)} \tag{2.2}$$

where $I_k(r,\phi,z)$ is the intensity distribution of the beam inside the fiber, then the rate equation for the density of electrons n_2 in the upper state and optical power of

the beams P_k can be expressed as

$$\frac{dn_2}{dt} = \sum_{k=1}^{m} \frac{P_k i_k}{h\nu_k}\sigma_k^a n_1(r,\phi,z) - \sum_{k=1}^{m} \frac{P_k i_k}{h\nu_k}\sigma_k^e n_2(r,\phi,z) - \frac{n_2(r,\phi,z)}{\tau} \quad (2.3)$$

$$\frac{dP_k}{dz} = u_k\sigma_k^e \int_0^{2\pi}\int_0^{\infty} i_k(r,\phi)\, n_2(r,\phi,z)\, r dr d\phi\, (P_k(z) + mh\nu_k\delta\nu_k) \quad (2.4)$$
$$-u_k\sigma_k^a \int_0^{2\pi}\int_0^{\infty} i_k(r,\phi)\, n_1(r,\phi,z)\, r dr d\phi\, (P_k(z))$$

where τ is the spontaneous lifetime (~12ms) of Erbium, u_k is the direction of the propagating beams (1 for forward, -1 for backward), $\sigma_k^{e,a}$ is the emission (absorption) crosssection, and n_1 is the density of elctrons in the ground state. $mh\nu_k\delta\nu_k$ represents the energy from spontaneous emission within the bandwidth of $\delta\nu_k$ at λ_k with m (m between 1 and 2) as the contributions from two different polarization.

If one defines $b_{eff} = \left[\frac{1}{2}\int_0^{\infty}\frac{n_t(r)}{n_t(0)} r dr d\phi\right]^{\frac{1}{2}}$ as the effective radius of doping profile, $\bar{n}_i(z) = \frac{1}{\pi b_{eff}^2}\int_0^{2\pi}\int_0^{\infty} n_i(r,\phi,z)\, r dr d\phi$ as the average electron density after the spatial averaging (i = 1, 2, t for ground state, excited state and total density of electrons), and $\Gamma_{k,i}(z) = \frac{1}{\bar{n}_i(z)}\int_0^{2\pi}\int_0^{\infty} i_k(r,\phi)\, n_i(r,\phi,z)\, r dr d\phi$ as the overlap integral between the optical beam and doping profile, then rate equations can be reduced in the following simple forms.

$$\frac{d\bar{n}_2}{dt} = \sum_{k=1}^{m} \frac{P_k}{h\nu_k\pi b_{eff}^2}\left(\sigma_k^a\Gamma_{k,1}\bar{n}_1 - \sigma_k^e\Gamma_{k,2}\bar{n}_2\right) - \frac{\bar{n}_2}{\tau} \quad (2.5)$$

$$\frac{dP_k}{dz} = u_k(\alpha_k + g_k)\frac{\bar{n}_2}{\bar{n}_t}P_k(z) + u_k g_k\frac{\bar{n}_2}{\bar{n}_t}mh\nu_k\delta\nu_k - u_k(\alpha_k + l_k)P_k(z) \quad (2.6)$$

After applying the steady state condition ($\frac{d\bar{n}_2}{dt} = 0$) to get,

$$\frac{\bar{n}_2}{\bar{n}_t} = \frac{\sum_{k=1}^{m}\frac{P_k(z)}{h\nu_k\xi_k}\alpha_k}{1 + \sum_{k=1}^{m}\frac{P_k(z)}{h\nu_k\xi_k}(\alpha_k + g_k)} \quad (2.7)$$

it is possible to get the solution for the pump and signal inside the EDFA by using

experimental parameters (such as the absorption $\alpha_k(\lambda) = \sigma_k^a \Gamma_{k,1}(\lambda) n_t$, gain $g_k(\lambda) = \sigma_k^e \Gamma_{k,2}(\lambda) n_t$ and saturation parameter $\xi = \frac{\pi b_{eff}^2 \bar{n}_t}{\tau}$).

The typical doping concentration ranges from 10 to 1000 ppm [22], and the required EDF length to get the 40dB of gain usually varies between 1 to 100 meters depending on the structure and doping concentrations of the fiber. The saturation input power is a function of the fiber structure, and have values typically around 1mW.

Figure 2.4 illustrates how these EDFA characteristics can be measured with an optical spectrum analyzer. By scanning a tunable light source (such as a fiber laser) and scaling the output of the EDFA, the gain as a function of signal wavelength, input level and pump power can be obtained at the same time. The noise figure can be calculated from the ASE level at the signal wavelength, using $P_{out} = GP_{in}$, and $N_{out} = 2n_{SP}(G-1)h\nu_0 B_0 + h\nu_0 B_0$ (P = signal, N = noise, B_0 = optical bandwidth, and 2 for polarization factor) [20],

$$F = \frac{\frac{S_{ASE}(\nu_0)}{h\nu_0} + 1}{G} \tag{2.8}$$

where S_{ASE} is the ASE power spectral density (W/Hz) and G is the gain of the amplifier. It is also possible to do these measurements without an optical spectrum analyzer, but a lock-in amplifier must then be used to reject ASE from the signal power measurement.

Figure 2.5 shows the measured gain of a typical EDFA. The doping concentration was 100ppm, and the fiber length was 12 meters. The calculated gain dependence on EDFA length is plotted in figure 2.6. It shows the existence of an optimum length

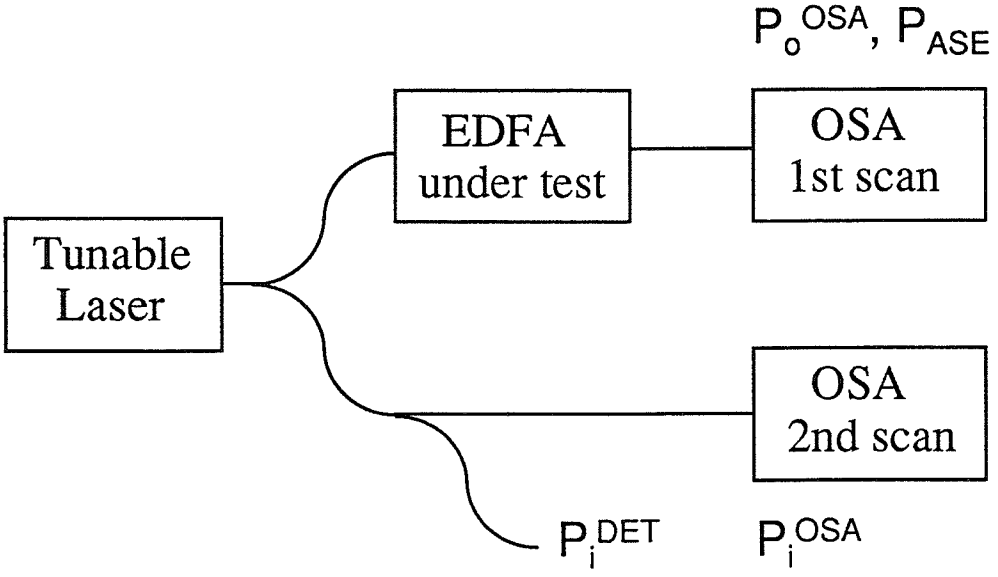

Figure 2.4: Use of an optical spectrum analyzer to characterize an EDFA.

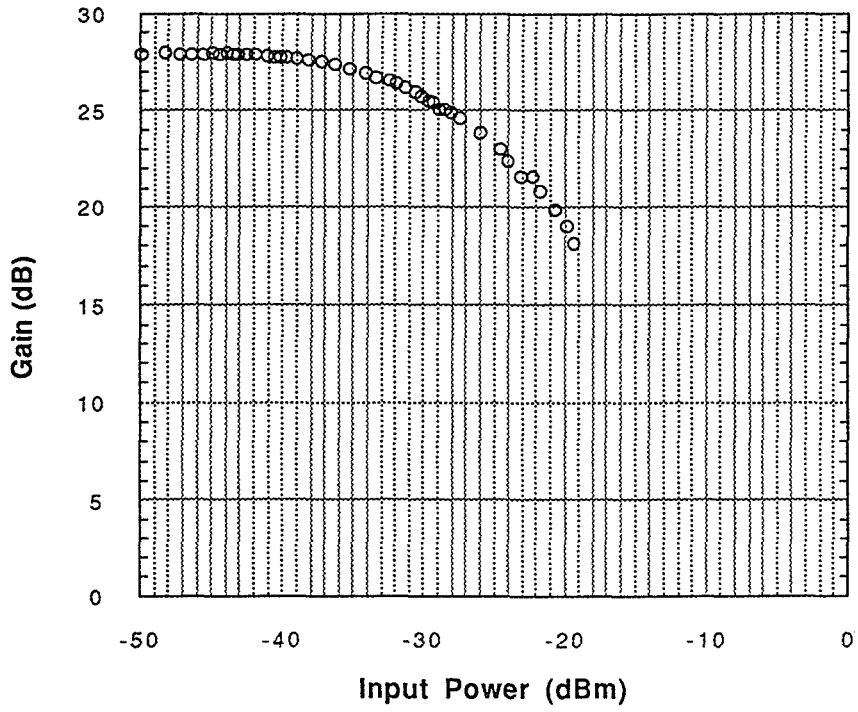

Figure 2.5: Measured gain for a 12meter piece of Erbium doped fiber (100ppm) at a pump power of 20mW. Signal wavelength = 1532nm.

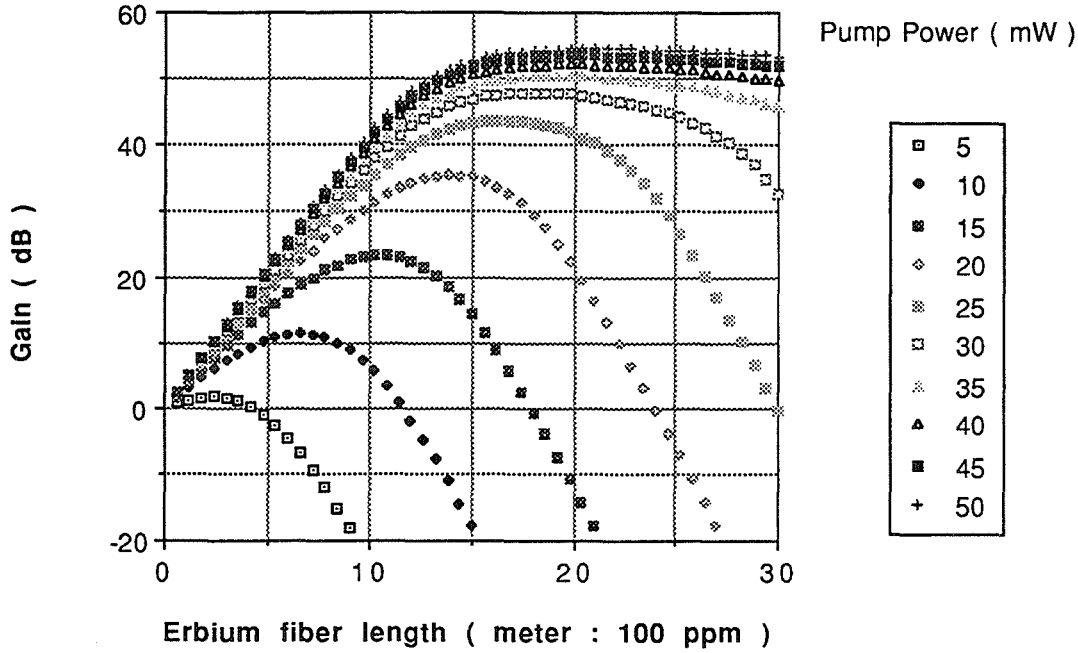

Figure 2.6: Theoretical plot of EDFA gain as a function of various parameters. The input parameters were determined from an independent experiment with the sample used in the figure 2.5.

for the EDFA, at a given pump power. If the fiber is too short, the pump power is wasted. If the doped fiber gets too long, then the end section of EDFA acts as an absorber and again reduces the efficiency of the amplifier.

Bibliography

[1] R. H. Stolen, and E. P. Ippen, Appl. Phys. Lett., **22**, 276 (1973)

[2] C. G. Atkins, D. Cotter, D. W. Smith, and R. Wyatt, Electron. Lett., **22**, 556 (1986)

[3] T. L. Koch, and U. Koren, IEEE J. Quantum Electron., **27**, 641 (1991)

[4] G. Eisenstein, R. S. Tucker, J. M. Wiesenfield, P. B. Hansen, G. Raybon, B. C. Johnson, T. J. Bridges, F. G. Storz, and C. A. Burrus, Appl. Phys. Lett., **54**, 454 (1989)

[5] S. B. Poole, D. N. Payne, and M. E. Ferman, Electron. Lett. **21**, 737 (1985)

[6] M. Wada, K. Yoshino, M. Yamada, and J. Temmyo, Photon. Tech. Lett. **3**, 953 (1991)

[7] C. R. Giles, and E. Desurvire, J. Light. Technol., **9**, 147 (1991)

[8] G. R. Walker, N. G. Walker, R. C. Steele, M. J. Creaner, and M. C. Brain, J. Light. Technol., **9**, 182 (1991)

[9] K. Tajima, M. Ohashi, and Y. Sasaki, J. Light. Technol., **7**, 1499 (1989)

[10] D. B. Mortimore, J. Light. Technol., **6**, 1217 (1989)

[11] C. M. Miller, and J. W. Miller, Electron. Lett. **28**, 216 (1992)

[12] G. A. Ball, W. W. Morey, and W. H. Glenn, Photon. Tech. Lett., **3**, 613 (1991)

[13] D. B. Patterson, A. A. Godil, G. S. Kino, and B. T. Khuri-Yakub, Opt. Lett., **14**, 613 (1989)

[14] M. Asobe, T. Kanamori, and K. Kubodera, Photon. Tech. Lett., 4, 362 (1992)

[15] R. I. Laming, R. L. Reekie, and D. N. Payne, Electron. Lett. **25**, 455 (1989)

[16] S. G. Grubb, W. H. Humer, R. S. Cannon, S. W. Vendetta, K. L. Sweeney, P. A. Leilabady, M. R. Keur, J. G. Kwaswgroch, T. C. Munks, and D. W. Anthon, N. Kagi, A. Oyobe, and K. Nakamura, Electron. Lett. **28**, 1275 (1992)

[17] E. Desurvire, C. R. Giles, J. L. Zyskind, J. R. Simpson, P. C. Becker, and N. A. Olsson, Proc. Optical Fiber Comm., **OFC 90**, (1990), paper FA1

[18] C. R. Giles, and E. Desurvire, J. Light. Technol., **9**, 271 (1991)

[19] A. A. M. Saleh, R. M. Jopson, J. D. Evankow, and J. Aspell, Photon. Tech. Lett. **2**, 714 (1990)

[20] Hewlett Packard application briefs, section E

[21] W. H. Press, B. P. Flannery, S. A. Teukolsky, and W. T. Vetterling, Numerical recipes in Pascal, Cambridge University Press (1989)

[22] N. Kagi, A. Oyobe, and K. Nakamura, Photon. Tech. Lett. **2**, 559 (1990)

[23] R. G. Smart, J. L. Zyskind, J. W. Sulhoff, and D. J. DiGiovanni, Photon. Tech. Lett. **4**, 1261 (1992)

[24] Y. Ohishi, T. Kanamori, T. Nishi, and S. Takahashi, Photon. Tech. Lett. **3**, 715 (1991)

[25] S. B. Poole, Optical Fiber Comm., **OFC 94**, (1994), tutorial WE

Chapter 3

Fiber Lasers

Using an EDFA as a gain element, it is straightforward to construct a laser by providing appropriate feedback elements such as a mirror, fiber Bragg grating, or fiber optic coupler in a ring resonator. This chapter will discuss the conception, construction, and basic characteristics of single frequency fiber ring laser developed at Caltech. Later chapters will be dedicated to the discussion of its noise characteristics and its applications.

3.1 Single mode fiber lasers

Achieving single mode operation in the fiber laser is more difficult than for the case of other lasers, since the distributed gain (few dB per meter) in an EDFA forces the resonator length of the laser to be large. For example, a meter of standing wave fiber resonator gives a free spectral range of 100MHz, which corresponds to a hundredth of a nanometer. The large gain bandwidth (around 50nm) of the EDFA, when combined

with these densely spaced longitudinal modes, causes the laser to operate with many longitudinal modes. In addition, spatial hole burning also acts against the single mode operation of the laser in the case of a standing-wave resonator.

Still, there exist several ways to achieve single mode lasing action in an Erbium doped fiber laser. The first approach demonstrated employed a coupled resonator (Smith-Fox configuration) to achieve an effectively larger free spectral range [3]. Even though it was possible to achieve single frequency operation, it was difficult to control the lasing wavelength. Also, the individual resonator lengths had to be controlled precisely to maintain single mode operation. More direct and recent approaches include fiber Bragg grating based laser. The fiber Bragg grating can be written directly onto the Erbium fiber using UV source holography [4]. By adjusting the pitch and depth of the UV induced index grating, it is possible to adjust the Bragg reflection band center wavelength and bandwidth (0.1nm $\sim$ 25nm). Even though it is possible to make single mode laser by applying this filter inside a short cavity, the tuning range cannot go beyond a few nanometers, and restricts its usage [5]. Using other types of tunable filters in the standing wave resonator is again difficult due to their high insertion loss, which forces the use of longer fiber gain lengths. Unless the bandwidth of the filter is narrow enough, spatial hole burning then limits the single mode operation of the laser again.

3.2 Erbium doped fiber ring lasers (EDFRL)

Figure 3.1 illustrates the concept of spatial hole burning. Different waves which satisfy the boundary condition of the standing wave resonator create different intensity distribution profiles inside the gain medium. Due to the difference in the intensity profile in space, different waves derive stimulated emission from Erbium ions at different locations inside the Erbium fiber. Specifically, with one mode lasing inside the resonator, undepleted Erbium ions at the antinode of the wave will support other modes which have their intensity nodes at the position of the undepleted Erbium ion. In this way, a standing wave resonator with a distributed gain medium have a higher tendency to operate as a multimode laser [6].

The usual way to get around the spatial hole burning problem is to employ a ring resonator for the laser. With the travelling wave inside the resonator, the distributed Erbium ions in the Erbium fiber experience almost uniform beam intensity through its length, and the position-dependent gain-eating problem of standing wave resonator can be avoided. Using this idea, the first fiber ring laser was able to demonstrate single mode operation with restricted performance [7]. Later versions included tuning elements such as acousto-optic [8] or liquid crystal tunable filters [9], but all of them had to suffer from severe mode hopping, due to the excessively wide bandwidth ($\sim$ 10GHz) of the widely tunable filters, compared to the densely spaced longitudinal modes of the laser ($\sim$ 10MHz).

The first truly stable single mode Erbium doped fiber ring laser (EDFRL) was demonstrated at Caltech [11]. With an additional narrow bandpass ($\sim$ 100MHz)

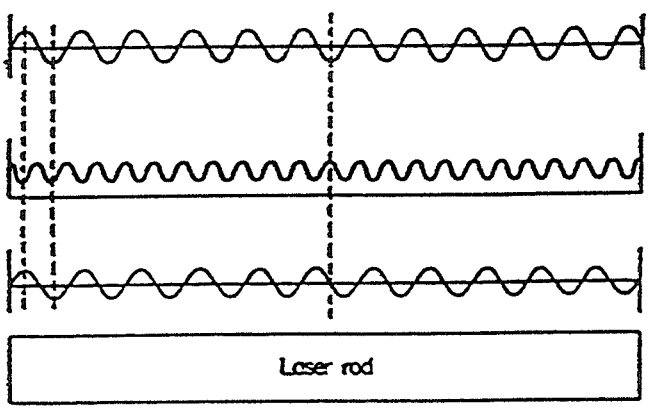

Figure 3.1: Figure illustrates two different waves which satisfy the boundary condition of the standing wave resonator. At the center of the gain medium, the Erbium ions contribute to the gain of upper mode while providing no gain to the mode in the bottom. At quarter wave shifted location, this situation is reversed.

fiber Fabry-Perot filter [10] within the passband of the tuning filter, it was possible to define the lasing frequency with more precision, suppressing the mode hopping behavior while retaining the tuning capability from the large bandpass filter.

Figure 3.2 illustrates the schematic diagram for the laser structure and the concept of cascaded FFP filters. The 980nm pigtailed laser diode (Lasertron, 65mW pump power in line) was spliced to a fused wavelength division multiplexer as a pumping source. The EDFA (Corning) was 15 meters long, and had 40dB of peak gain and 3mW of saturated ASE output power when pumped with 40 mW of 980nm pump. Pigtailed polarization independent isolators (E-Tek Dynamics, Isolation greater than 40dB) force the laser to operate in one direction preventing spatial hole burning. They also eliminate interactions between different elements inside the resonator, and block unwanted reflections from the output port of the system. A polarization controller (PC) [13] with a pigtailed polarizer [12] was used to control the polarization state of the laser, as well as to eliminate the competition between different polarization modes. The lasing wavelength was set by tuning the broadband fiber Fabry-Perot filter (FFP : bandwidth 26.1 GHz, FSR 4020 GHz, insertion loss 3dB from Micron optics). The second FFP with a smaller bandwidth (1.39 GHz) was put in to the resonator to suppresses the mode hopping. The threshold was around 15mW, depending on the lasing wavelength. The resonator length of the laser used in the characterization was 50 meters corresponding to a laser free spectral range (FSR) of 4MHz.

The laser output was coupled out from the resonator through a fused fiber optic coupler. The output power was approximately 1mW, depending on the wavelength

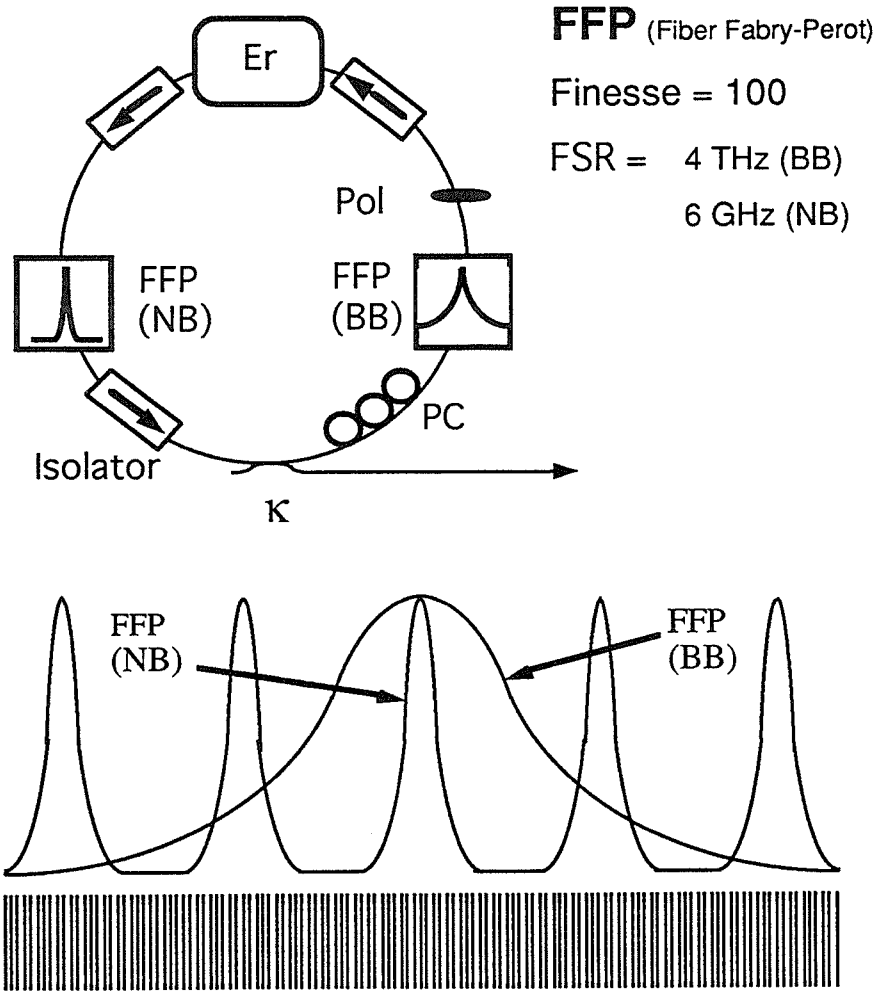

Figure 3.2: The upper picture illustrates the structure of an Erbium doped fiber laser used in the experiment. Lower picture shows the idea of a tandem fiber Fabry-Perot filter. The narrow bandpass filter selects the lasing mode from densely spaced laser resonator modes, and the broad band-pass filter sets the lasing wavelength.

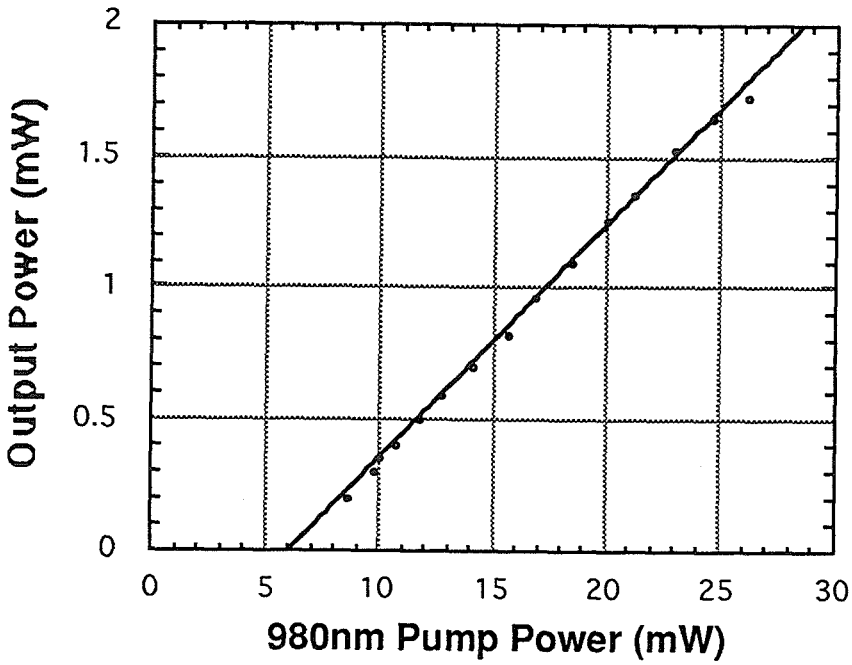

Figure 3.3: Figure of laser output power versus pump power. Lasing wavelength = 1532nm.

and pump power. Figure 3.3 shows the output power of the laser as a function of pump power at the lasing wavelength of 1532nm.

Figure 3.4 shows a lasing spectrum taken using the scanning Fabry-Perot Interferometer (Newport Research Super-resonator SR-170. FSR 6 GHz. finesse 6000). This device has a resolution of 1 MHz which is sufficient to resolve the 4 MHz FSR of the ring laser longitudinal modes. The displayed picture shows only one visible peak in 12.5 MHz/Division scan, confirming the single mode operation of the laser. Tuning can be achieved by either changing the voltage to the broadband FFP thus scanning the center frequency of the FFP over transmission peaks of a narrowband FFP (for the coarse tuning), or by applying DC voltage to the narrowband FFP to scan the center

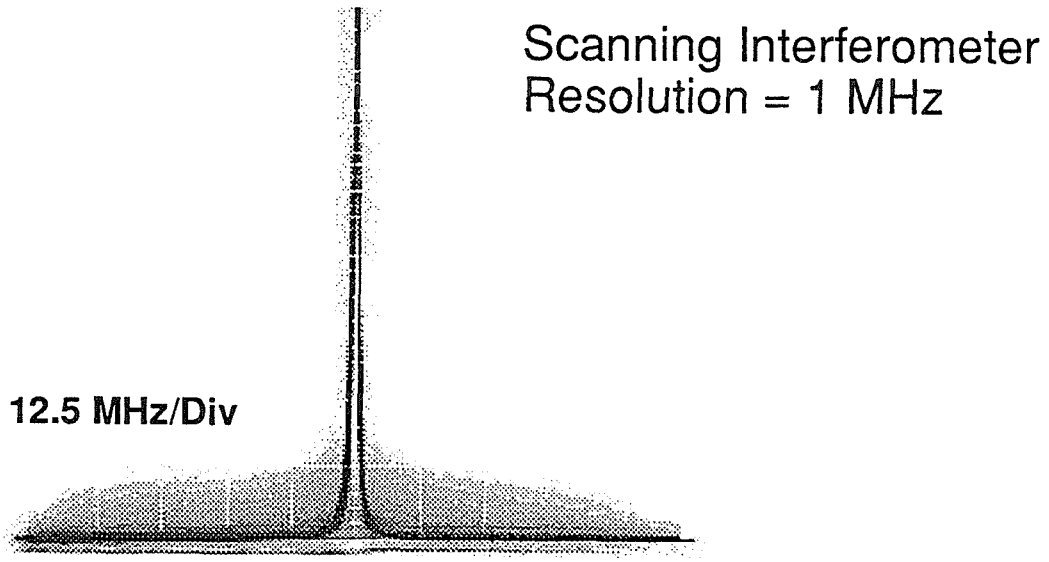

Figure 3.4: This picture shows the lasing spectrum taken from the high resolution Super resonator scanning interferometer. The resolution of the device is less than 1MHz, and the resonator mode spacing of the laser is 4MHz.

frequency of the narrowband FFP over the different longitudinal resonator mode of the ring laser (fine tuning. See figure 3.2). Figure 3.5 shows one of the tuning curves as a function of the PZT Voltage applied to the broadband FFP. Tuning over 30nm (corresponding to the FFP filter FSR) between 1530nm to 1560nm was possible by applying 0 to 17 DC Volts. The tuning range can be extended by using a broadband FFP filter with larger FSR. After 17 Volts, the wavelength retraces at zero applied Voltage.

Even though weak sidemodes are not visible in the scanning interferometer trace in figure 3.4, these modes do exist and must be characterized. The sidemode suppression ratio can be measured by scaling the power of the beating signal between the main mode and a side mode produced in the photodetection, relative to the main mode optical power. Since the sidemode suppression ratio is a function of the loss difference between the main mode and the side mode inside the resonator ($\frac{P_m}{P_0} = \frac{(\alpha_m - \alpha_0)P_0}{\theta}$, $\theta =$ spontaneous emission rate, $\alpha_m =$ cavity loss at the mth side mode) [14], it is possible to increase the sidemode suppression ratio (figure 3.6) by controlling either the shape of the mode selection filter or the mode spacing of the laser.

Using DC current meter to measure the main mode optical power, and a microwave spectrum analyzer to measure the size of the photocurrent beating signal, SMS was measured with different combinations of resonator mode spacing and FFP bandwidth. The size of the SMS varied from 38dB (with 4MHz laser FSR and 1300MHz bandpass filter) to 70dB (with 10MHz mode spacing and a 50MHz bandpass filter).

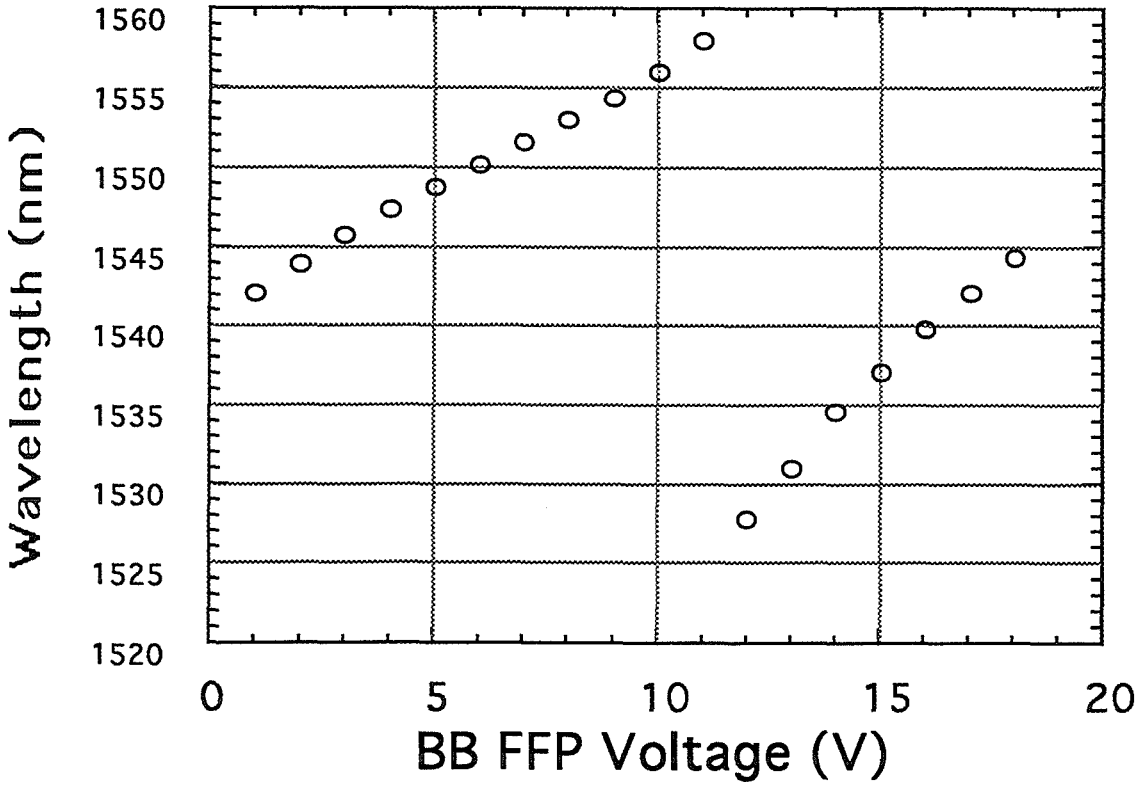

Figure 3.5: This graph shows one of the tuning curves for the ring laser. By applying 0 to 17 DC Volts to the piezoelectric tuning element in the FFP, it is possible to tune the laser over 30nm.

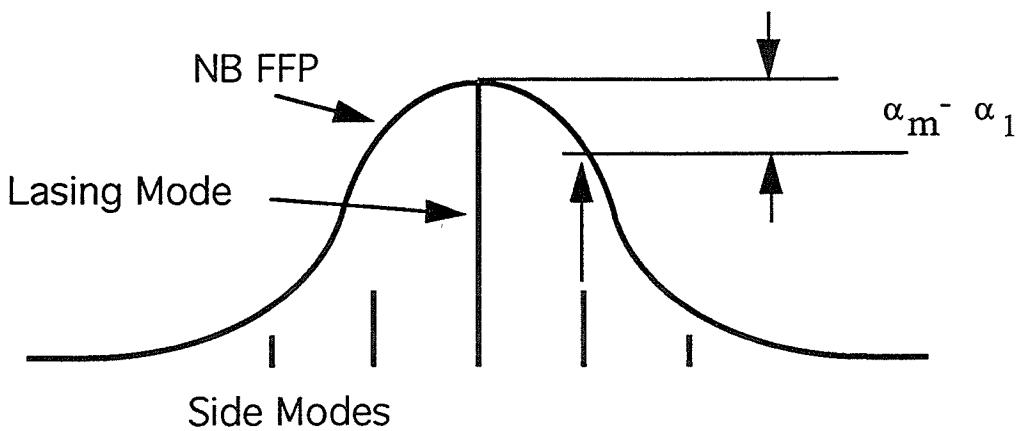

Figure 3.6: The sidemode suppression of a laser can be adjusted by changing the loss difference between the lasing mode and side mode inside the laser resonator. This can be achieved either by changing mode spacing or shape of the frequency selection element.

Bibliography

[1] G. J. Kintz, and T. Baer, IEEE J. Quantum Electron., **26**, 1457 (1990)

[2] K. Hsu, C. M. Miller, J. T. Kringlebotn, E. M. Taylor, J. Townsend, and D. N. Payne, Proc. Optical Fiber Comm., **OFC 94**, (1994), paper PD1

[3] P. Barnsley, P. Urquhart, C. Miller, and M. Brierley, J. Opt. Soc. Am. A, **5**, 1339 (1988)

[4] G. A. Ball, W. W. Morey, and W. H. Glenn, Photon. Tech. Lett., **3**, 613 (1991)

[5] G. A. Ball, and W. W. Morey, Opt. Lett., **17**, 420 (1992)

[6] C. L. Tang, H. Statz, and G. deMars, J. Appl. Phys., **34**, 2289 (1963)

[7] P. R. Morkel, G. J. Cowle, and D. N, Payne, Electron. Lett., **26**, 632, (1990)

[8] D. A. Smith, M. W. Maeda, J. J. Johnson, J. S. Patel, M. A. Saifi, and A. V. Lehman, Opt. Lett., **16**, 387 (1991)

[9] M. W. Maeda, J. S. Patel, D. A. Smith, C. Lin, M. A. Saifi, and A. V. Lehman, Photon. Tech. Lett., **2**, 787 (1990)

[10] C. M. Miller, and J. W. Miller, Electron. Lett. **28**, 216 (1992)

[11] N. Park, J. Dawson, K. Vahala and C. Miller, Appl. Phys. Lett., **59**, 2369, (1991)

[12] M. N. Zervas, Photon. Tech. Lett., **2**, 787 (1990)

[13] H. C. Lefevre, Electron. Lett. **25**, 597 (1990)

[14] G. P. Agrawal, and N. K. Dutta, Long-wavelength Semiconductor Lasers, A Van Nostrand Reinhold Book, (1986)

Chapter 4

Noise Characteristics of the EDFRL

The long spontaneous lifetime of Erbium ions and the long resonator length give the EDFRL unique intensity noise characteristics. The first half of this chapter will be dedicated to the discussion of the intensity noise characteristics, measurement and noise reduction techniques. The latter half of this chapter will describe the frequency noise of an EDFRL, including linewidth and frequency jitter. An analysis will be given to the special version of the self-heterodyne interferometer which was developed for the sub kHz linewidth measurement.

4.1 Intensity noise

4.1.1 Theory

When a laser is used as a transmitter, its intensity noise acts as a source of error. In sensing applications, the laser intensity noise can also restrict the resolution of the measurement. There have been intensive studies performed concerning sources of intensity noise [1]. Qualitatively, the relative intensity noise (RIN) spectral density function computed from the rate equations driven by spontaneous emission is given by,

$$RIN\,(\Omega) = \frac{1/\tau_R^2 + \Omega^2}{\left(w_R^2 - \Omega^2\right)^2 + \Omega^2/\tau_R^2}\Delta w_{ST} \tag{4.1}$$

where Ω is the frequency of the noise , w_R is the relaxation oscillation frequency, τ_R is the relaxation oscillation damping time, and Δw_{ST} is the Schawlow-Townes linewidth of the laser [9]. For a directly detected field, the RIN corresponds to the ratio of the mean square power per unit bandwidth of fluctuating photocurrent to the average photocurrent power. There exist two important features in this equation. First, the magnitude of RIN decreases at 20dB per decade in the high frequency regime ($\Omega \rightarrow \infty$). Second, the spectrum has a resonance at the relaxation oscillation frequency ω_R.

$$w_R = \sqrt{\frac{r-1}{\tau\, t_c}} \tag{4.2}$$

With appropriate values of $r = P/P_{th}$ (pumping factor $\sim$ 2, P_{th} = threshold pump power), t_c (photon lifetime inside the passive cavity $\sim$ 1μs.), and τ (spontaneous lifetime of Erbium ions $\sim$ 12ms.), the relaxation oscillation frequency has a value

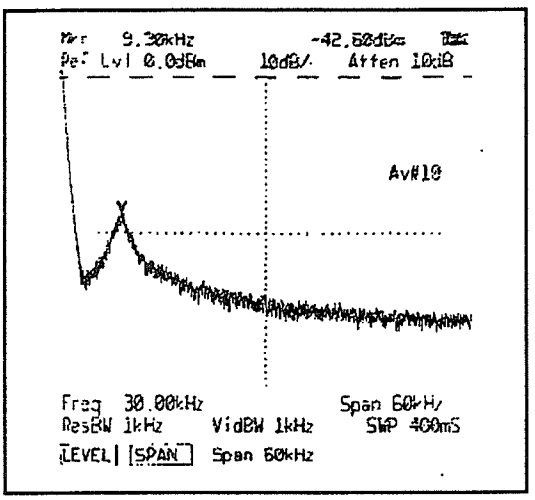

Figure 4.1: Measured relaxation oscillation frequency spectrum from a spectrum analyzer. The measured 10kHz agrees with the calculated value.

around 10kHz. Using equation 4.1 together with the measured relaxation oscillation frequency spectrum, it is possible to estimate the noise level at high frequencies. For example, figure 4.2 shows the calculated intensity noise between 1Hz and 1GHz, which was estimated with the measured relaxation oscillation spectrum shown in figure 4.1 (measured with a low corner frequency bias T and 48dB gain tandem amplifier). Figure 4.2 also illustrates the shot noise floor, which is a theoretical limit of the intensity noise (determined by the uncertainty relation between the photon number and phase, unless other noise reduction scheme applied), at optical power of 1mW. The calculated laser RIN reaches the shot noise floor after approximately 10MHz.

In reality, the laser noise spectrum shows more noise than is expected from this short analysis based on the case of ideal single mode laser. The actual measurement

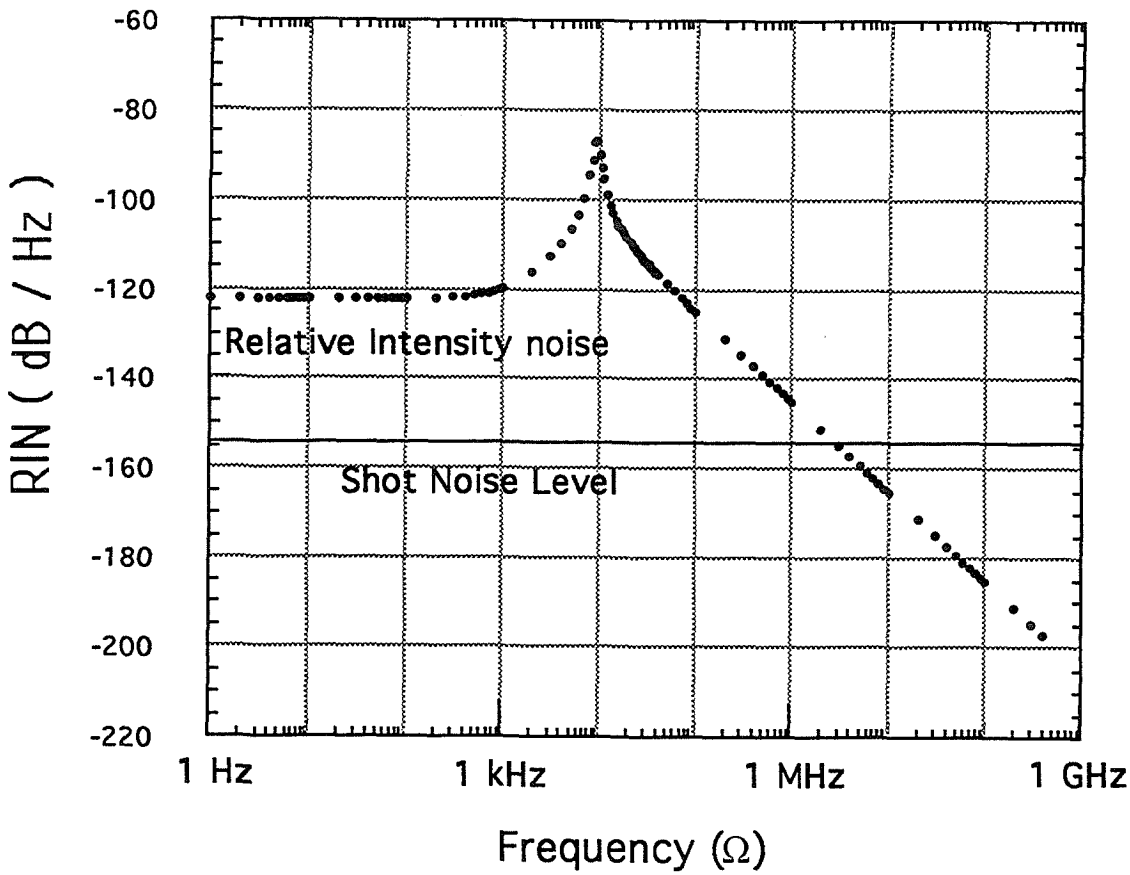

Figure 4.2: Expected relative intensity noise from an Erbium doped single mode fiber laser. The fitting parameters were obtained from the measurement of relaxation oscillation frequency in figure 4.1.

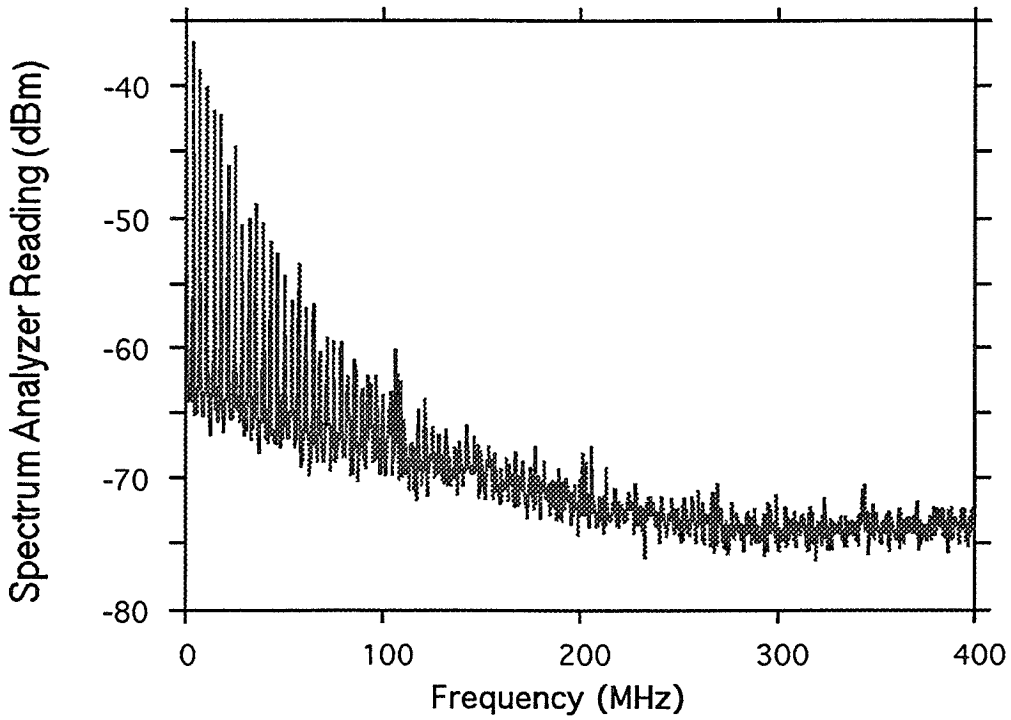

Figure 4.3: The beating noise spectrum of an EDFRL shows the existence of satellite side modes up to 400MHz. Resolution bandwidth of the spectrum analyzer = 300kHz.

(figure 4.3) shows the existence of periodic excess noise even up to 400MHz. The period of these variations (4MHz), which is identical to the FSR of the laser, indicates that the noise is from the beating between the main mode and remote sidemodes at the photodetector. Thus, to characterize the noise of the single mode fiber laser, it is necesary to consider the beating noise as well, even though the size of the sidemodes is negligible compared to the main mode.

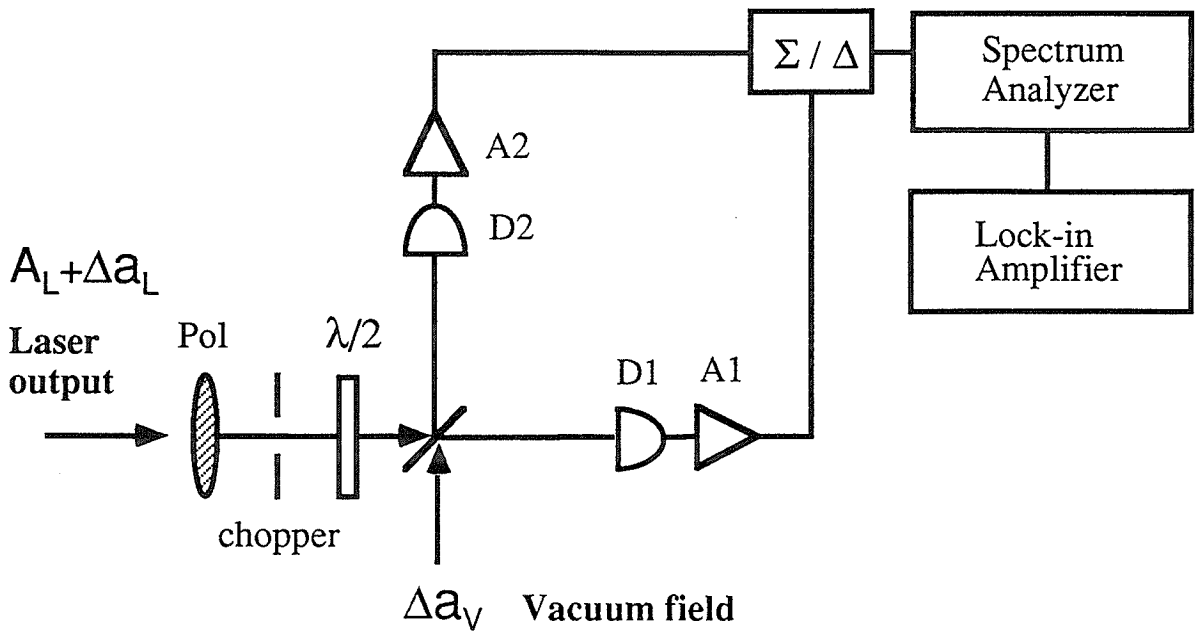

Figure 4.4: This picture shows the schematic diagram of the balanced homodyne detection system used in the noise measurement relative to the shot noise.

4.1.2 Balanced homodyne detection

Even though it is possible to estimate the amount of beating noise using the spectrum analyzer, the balanced homodyne detection system (BHD) should be used for a precise calibration of laser noise relative to the shot noise floor [5, 6]. By mixing the source to be measured with the vacuum field fluctuation using a beam splitter, one can exactly scale the laser noise in terms of vacuum fluctuations (shot noise). Figure 4.4 shows the schematic representation of the detection system. Due to the intrinsic phase difference $\frac{\pi}{2}$ between the transmitted beam and the reflected beam from the beamsplitter, the detected photocurrent at two different arms of the detection system

contain different AC components

$$I_1 \sim (A_L + \Delta a_L + \Delta a_V)^2/2 \sim A_L(\Delta a_L + \Delta a_V) + DC \quad (4.3)$$

$$I_2 \sim (A_L + \Delta a_L - \Delta a_V)^2/2 \sim A_L(\Delta a_L - \Delta a_V) + DC \quad (4.4)$$

where A_L is the DC amplitude of the laser output field, and $\Delta a_{L,V}$ is the field fluctuation of the laser (or vacuum). By summing or taking the difference of these currents at the hybrid junction (see figure 4.4), and measuring the power spectral density with a microwave spectrum analyzer, it is possible to measure the following quantities.

$$\left\langle (I_1 + I_2)^2 \right\rangle \sim A_L^2 \left\langle (\Delta a_L)^2 \right\rangle \quad (4.5)$$

for the laser noise (in the sum mode), and

$$\left\langle (I_1 - I_2)^2 \right\rangle \sim A_L^2 \left\langle (\Delta a_V)^2 \right\rangle \quad (4.6)$$

for the shot noise (in the difference mode). By dividing equation 4.5 by equation 4.6, it is possible to exactly scale the amount of laser noise in terms of shot noise.

4.1.3 Measurement

In the experiment, the laser was tuned to the gain peak of the EDFA by applying a DC voltage to the broadband FFP. Before the measurement, the BHD was balanced to greater than 55 dB using a modulated semiconductor laser at the measurement frequency, and adjusting the path length of two arms while monitoring the difference of the photocurrents of detector 1 and detector 2 (D1,D2. BT&D PDH0004. 50μm active region, bandwidth 2.4GHz) at the spectrum analyzer (Tek2782, 33GHz). Ninety percent of the laser output was then coupled to the BHD to measure the noise power

spectral density. Ten percent of the laser output was coupled to a Super-Cavity scanning Fabry-Perot interferometer to monitor the operation of the laser during the noise measurement. A polarization controller and polarizer were placed before the BHD to maintain a constant polarization into the BHD. The shot noise floor was determined by subtracting the amplified photocurrents of D1 and D2. The amplifiers had 52dB of gain with 3.7dB of noise figure (Avantek ACT10-213-1, 10MHz~1GHz). To confirm the shot noise level, shot noise was measured again with several different optical attenuators placed before the BHD with the laser power kept constant [5, 6]. By adding the amplified currents of D1 and D2, the noise power of the fiber laser was measured between 307 and 312 MHz at 500 kHz steps and using 300kHz resolution bandwidth in zero span mode of the spectrum analyzer. The measured laser intensity noise power was proportional to the laser output power, exhibiting a 3 dB periodic variation at 4 MHz intervals in frequency at the same laser output power (figure 4.5). The measured noise power was 8.5 dB above the shot noise level after the correction for the overall detection efficiency ($W_{obs} = \eta W + 1 - \eta$, η = overall efficiency, W = noise power [3]. with the 83% detector quantum efficiency and 56% loss between the laser and detector).

Knowing the noise is from the beating signal between the main mode and weakly excited sidemodes, it is possible to take several approaches to reduce the noise level. From the expression for the sidemode suppression ratio (using $\frac{dP_m}{dt} = gP_m - \alpha_m P_m + \theta$),

$$\frac{P_m}{P_0} = \frac{\theta}{(\alpha_m - \alpha_0)\, P_0} \qquad \left(\frac{dP_m}{dt} = 0 \; at \; steady \; state\right) \tag{4.7}$$

the first and most obvious approach to reduce beating noise is to use a better bandpass

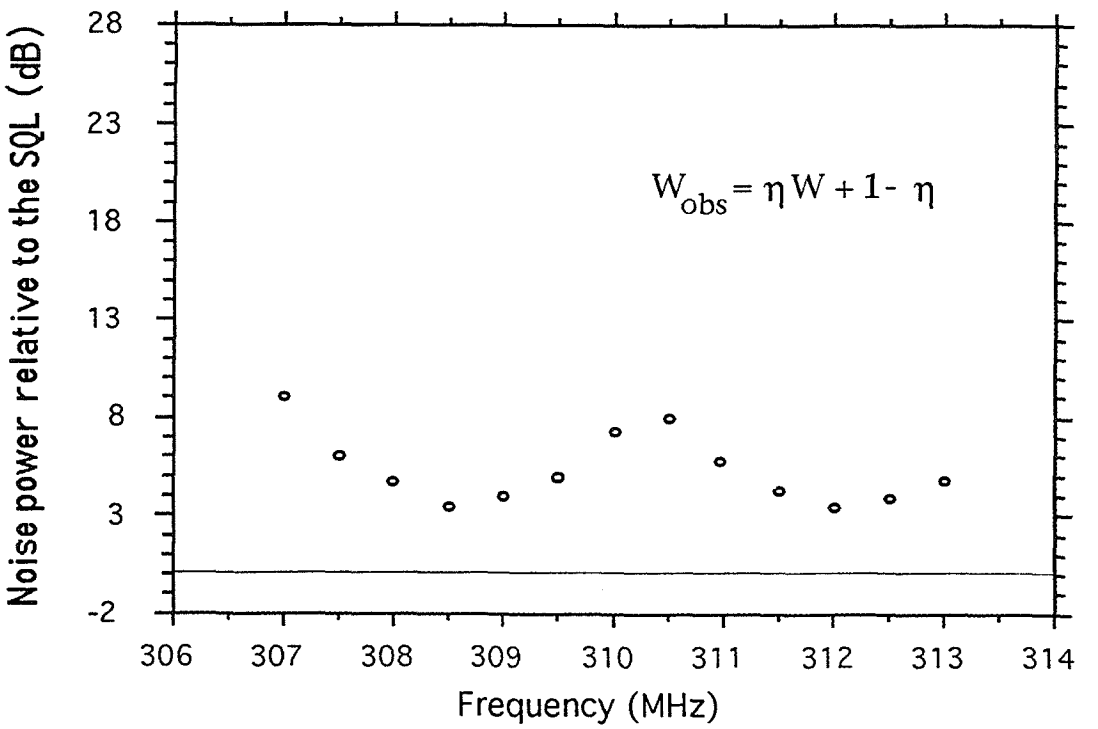

Figure 4.5: The measured noise spectrum of EDFRL around 300MHz. The noise shows a 4MHz periodic variation which is free spectral range of the laser.

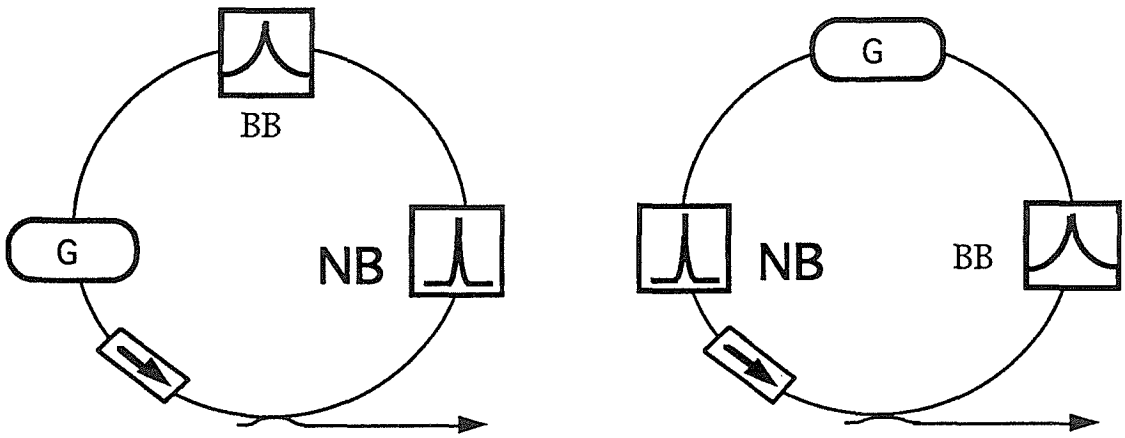

Figure 4.6: Comparison between the laser structure for a maximum output power operation and a proposed structure for the minimum noise operation.

filter to increase the loss difference between the main mode and sidemode (Here, P_m is the photon number of the mth side mode, θ is the spontaneous emission rate, and α_m is the loss of the passive cavity seen at the mth side mode wavelength).

A second and more fundamental approach to reducing the noise would be to decrease the spontaneous emission rate θ in equation 4.7 ($\theta = nG$, n = inversion factor, G = gain [10]), by decreasing cavity loss (G) or using a lower noise EDFA (such as with lower n).

Even though equation 4.7 seems to have only two parameters to adjust, there is a third and simpler way to reduce intensity noise by rearranging the structure of the laser. Figure 4.6 shows the proposed structure of the laser. By locating the frequency-selective narrow bandpass filter (FWHM=125MHz) between the gain module and the

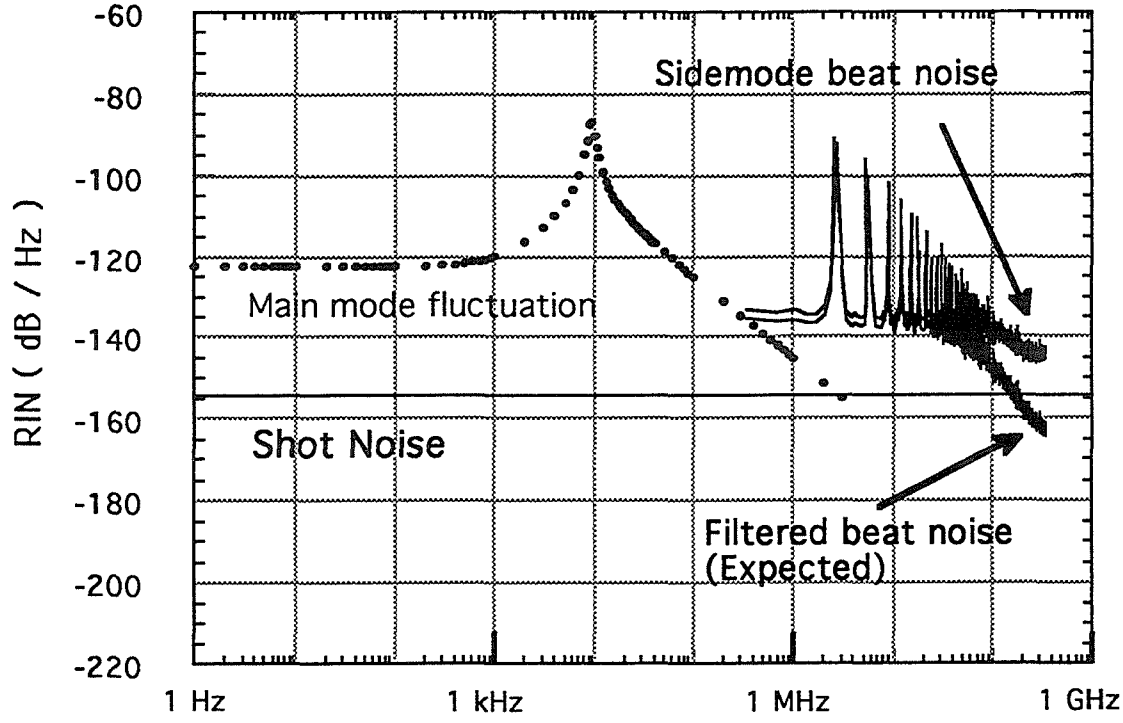

Figure 4.7: Calculated intensity noise with the proposed structure compared with the noise of maximum power configuration (see figure 4.6).

output coupler, it is possible to reduce the coupled output power of the satellite side mode by as much as 16dB at 300MHz. This in turn reduces the beating noise when the laser signal is detected. Figure 4.7 illustrates the expected amount of beating noise of the laser with and without the spectral filtering concept. With spectral filtering, it is expected that the laser will operate in the shot noise regime beyond 200MHz. (The power penalty for the main mode due to the intrinsic insertion loss of the FFP is 2dB and can be reduced if better coatings are employed for the filter). The measured noise power for this reduced noise configuration (see figure 4.8) agrees

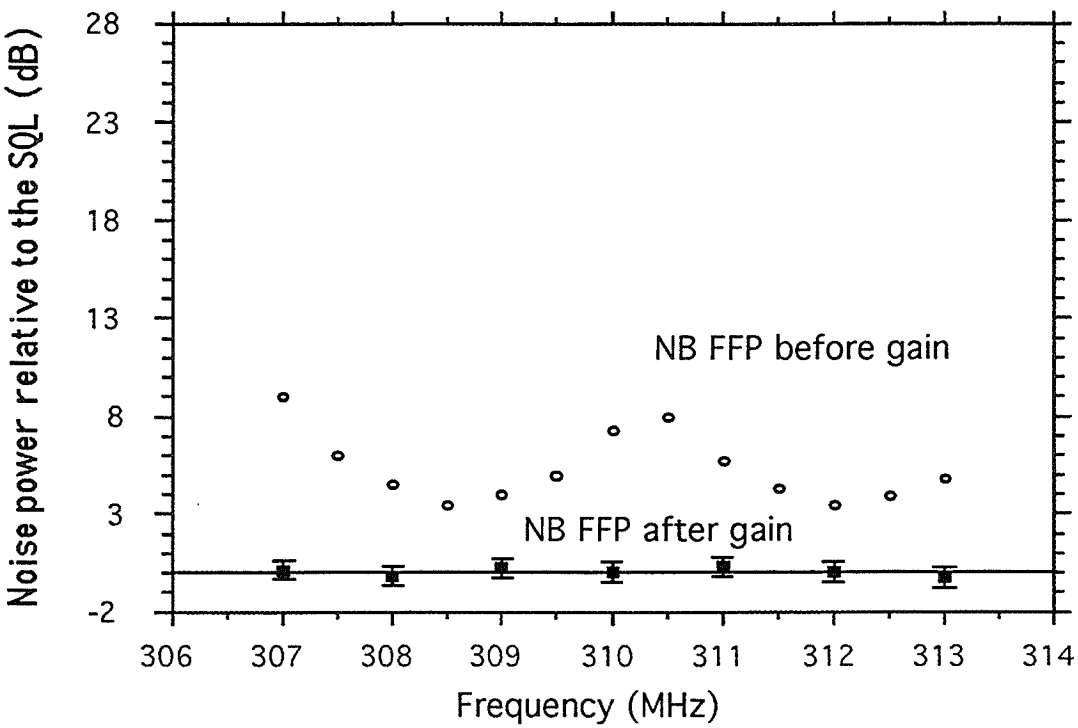

Figure 4.8: Measured intensity noise of the minimum noise configuration in comparison with maximum power configuration. Shot noise limited operation of the laser can be seen from the data.

with the estimation based on this concept, and shows shot noise limited behavior at around 300MHz.

To summarize, from DC to MHz range, the laser noise is dominated by the main mode fluctuation associated with the relaxation oscillation. From 1MHz to 1GHz, the main contribution to the laser noise results mainly from beating noise between the main mode and side mode, and shows oscillatory behavior with a period given by the laser FSR. Beyond 1GHz, the laser operates in the shot noise regime. In this

regime, the effect of the beating noise can be reduced by appropriately adjusting the laser structure.

4.2 Frequency noise

4.2.1 Theory

Linewidth and frequency stability of a laser are critical parameters for certain applications including coherent communication systems and coherent sensing systems. One of the most important advantages of the fiber laser compared to the semiconductor laser at this wavelength is its narrow linewidth. For example, in the expression for the laser linewidth (Schawlow and Townes [9]),

$$\Delta\nu_{ST} = \frac{h\nu_0 \left(\Delta\nu_{1/2}\right)^2}{P}\,\eta \tag{4.8}$$

the fiber laser have much smaller $\Delta\nu_{1/2}$ (full width of the passive cavity resonance, $\Delta\nu_{1/2} = \frac{c\left(\alpha - \frac{1}{l}\,ln\sqrt{R_1R_2}\right)}{2\pi n}$. η is the inversion factor, α is the distributed loss for the cavity, l is the cavity length, c is the speed of light, and R_i is the reflectivity of the mirrors) than the semiconductor laser due to its long cavity length. This leads to a theoretically estimated linewidth for the fiber laser easily below 1Hz with a cavity longer than 1 meter.

In a real system, the frequency noise of a laser is usually greater than kHz. Perturbations to the cavity caused by acoustic and thermal noise [9] usually occur at millisecond time scale, and induce fluctuations in the cavity length. This leads to the fluctuation in longitudinal modes of the resonator, and thus introduces jitter in the

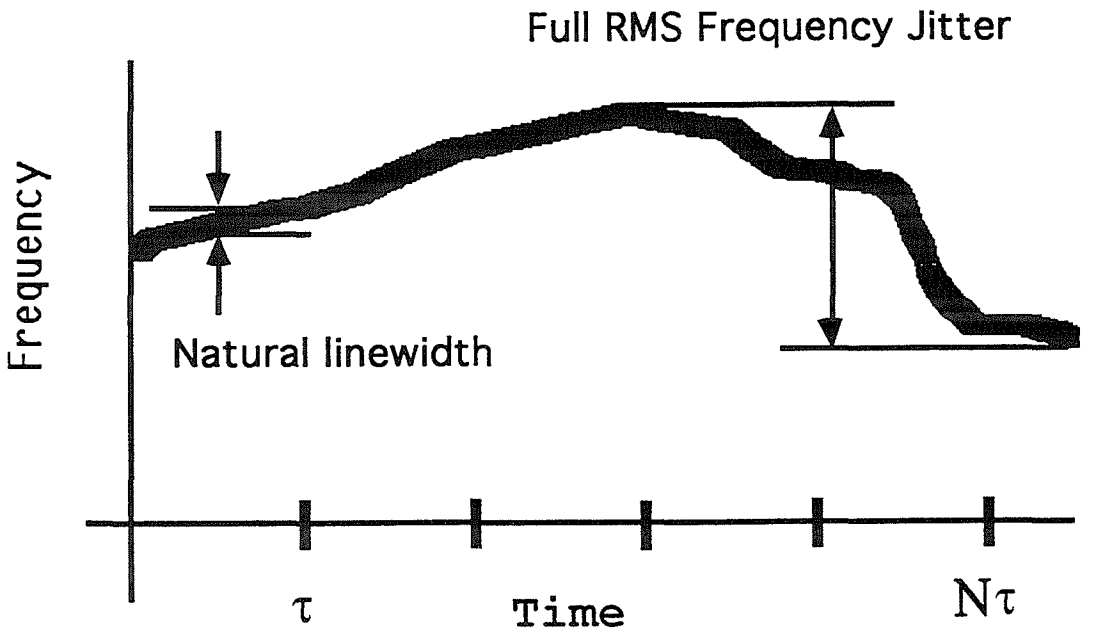

Figure 4.9: This figure illustrates the contribution of the frequency jitter and fundamental linewidth of the laser to the overall linewidth of the laser.

lasing frequency. For a narrow linewidth source such as fiber laser, this phenomenon makes frequency jitter dominate over the natural linewidth (figure 4.9).

4.2.2 Recirculating DSHI

For the measurement of laser linewidths, the delayed self-heterodyne interferometer (DSHI) has been used as a standard tool (figure 4.10) [16] . However, the requirement that the delay line, L_D,to be larger than the coherence length of the laser, L_C,

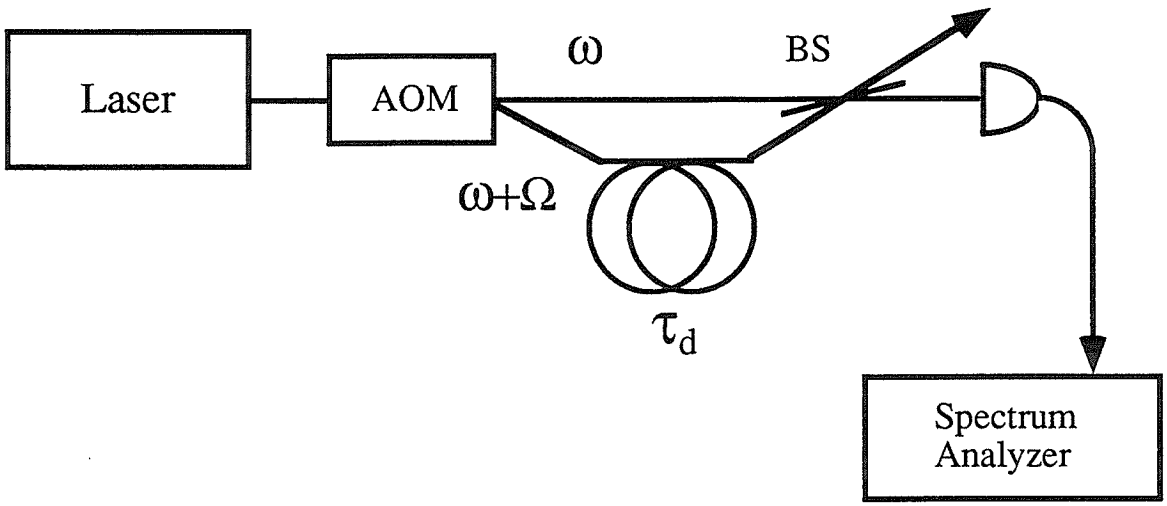

Figure 4.10: Schematic of a self heterodyne interferometer for linewidth measurement. The delay line length should be longer than the coherence length of the laser to decorrelate the frequency shifted beam.

has limited the use of this interferometer to relatively broad linewidths sources. For narrow linewidth lasers, linewidths have been indirectly derived by fitting the measured spectra to the theoretically calculated spectra [11]. Still, this is not a precise way to measure the linewidth of a laser. To circumvent this problem, the concept of a recirculating loop delay was introduced [12]. By placing a delay line and frequency shifting element (acousto optic modulator) inside a recirculating loop, it was possible to effectively increase the length of the delay line, by counting the number of recirculations using the total accumulated frequency shift of the beating signal in the spectrum analyzer. However, the resolution enhancement by this approach was limited to only a factor of 3 or less (i.e., 3 round-trips), mainly due to the large loss

inside the recirculating loop.

This problem of signal fading in the interferometer can be overcome if the loss inside the recirculating loop is compensated. For wavelengths around 1.5μm, this can be done using an EDFA. At other wavelengths, other types of optical amplifier can be used.

In the resulting loss-compensated recirculating delay loop, it is necessary to consider multiple contributions to the kth-order beat note on the spectrum analyzer. Specifically, the laser output that has been delayed n + k times in the loop can beat with a signal field that has been delayed n times, adding a contribution to the kth-order beat-note. However, if $k\tau_D$ is greater than the laser coherence time, and if the laser frequency is fixed over $n\tau_D$, then each of these contributions will contribute the same signal lineshape when detected as a beating signal in the spectrum anayzer.

Figure 4.11 shows the layout of the improved interferometer developed in Caltech for the ultranarrow linewidth measurement of an EDFRL. The loop consists of 11 km of standard transmission fiber and an acousto-optic modulator (AOM : 10 percent efficiency, operated at 140 MHz.). Each pass through the recirculator thereby delays the optical beam in time and introduces a 140 MHz frequency shift. After completion of a pass, 10% of the light is coupled out of the loop and heterodynes with the directly transmitted wave at the detector (Ortel 2515B, 16GHz response). The other 90% is recoupled into the loop for further delay and frequency shifting. Spectrum analysis of the detected photocurrent therefore shows a series of frequency-shifted peaks corresponding to photomixed beatnotes produced by the directly transmitted

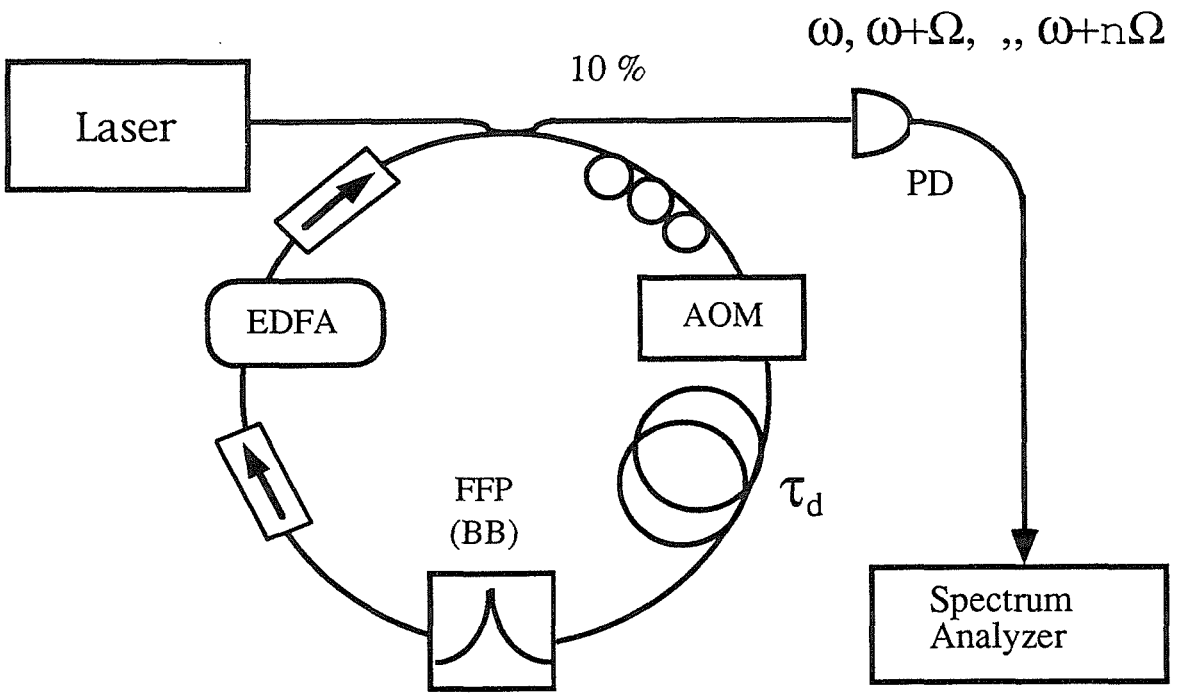

Figure 4.11: Loss-compensated recirculating delayed self heterodyne interferometer for the ultra-narrow linewidth measurement. By placing the frequency shifter and delay line inside the circulating loop, it is possible to effectively increase the delay line length while monitoring the number of recirculations.

wave mixing with increasingly-delayed, frequency-shifted waves. An EDFA was placed after the elements such as AOM, delay line, FFP bandpass filter, and optical isolator, to avoid the saturation of EDFA gain from the large input signal from the laser, while compensating the loss from these elements. A FFP bandpass filter (bandwidth 42 GHz, finesse = 100) and a pigtailed optical isolator are also included in the RDSHI to reduce the recirculating amplified spontaneous emission and to inhibit loop oscillation. By adjusting the pump power of the RDSHI gain module and matching the bandpass filter wavelength of the RDSHI to the ring laser wavelength, it was possible to detect the recirculated beam delayed as many as 70 roundtrips through the loop (figure 4.12), without any unintentional recirculator oscillation [13].

To test for the possibility of spectral broadening due to the erbium amplifier [14], the 11 km delay line was removed from the RDSHI. Figure 4.13 (a), (b) and (c) show the beatnotes at 1st, 20th and 30th orders, without the delay line. The maximum observed broadening was less than 400 Hz indicating that spectral broadening from the amplifier alone should not interfere with our measurement (the resolution limit of which is 606 Hz at 30 orders with the 11 km delay line). For a further check, the FWHM linewidth for the first three orders were measured both with and without the amplifier in place (figure 4.14). A difference in linewidth between the system with the amplifier and the system without the amplifier was not observed. Again, a large improvement in signal to noise ratio can be seen from the picture.

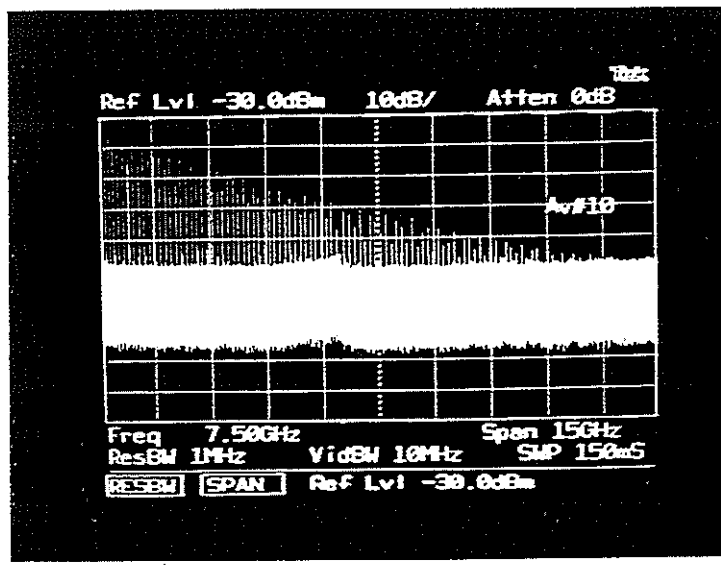

Figure 4.12: The beating spectrum taken from the output of an RDSHI. The spectrum shows the existence of the beating signal which has circulated through the delay line up to 70 times.

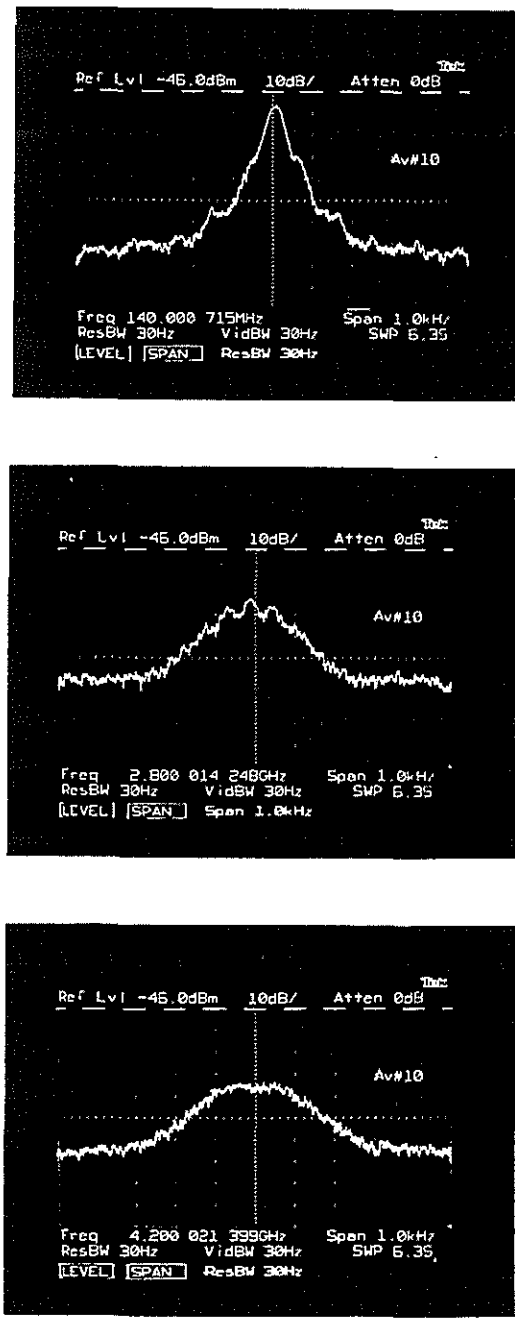

Figure 4.13: The beating spectra taken at the 1st, 20th, and 30th pass through the EDFA without the delay line. The linewidth broadening was measured to be less than 400Hz.

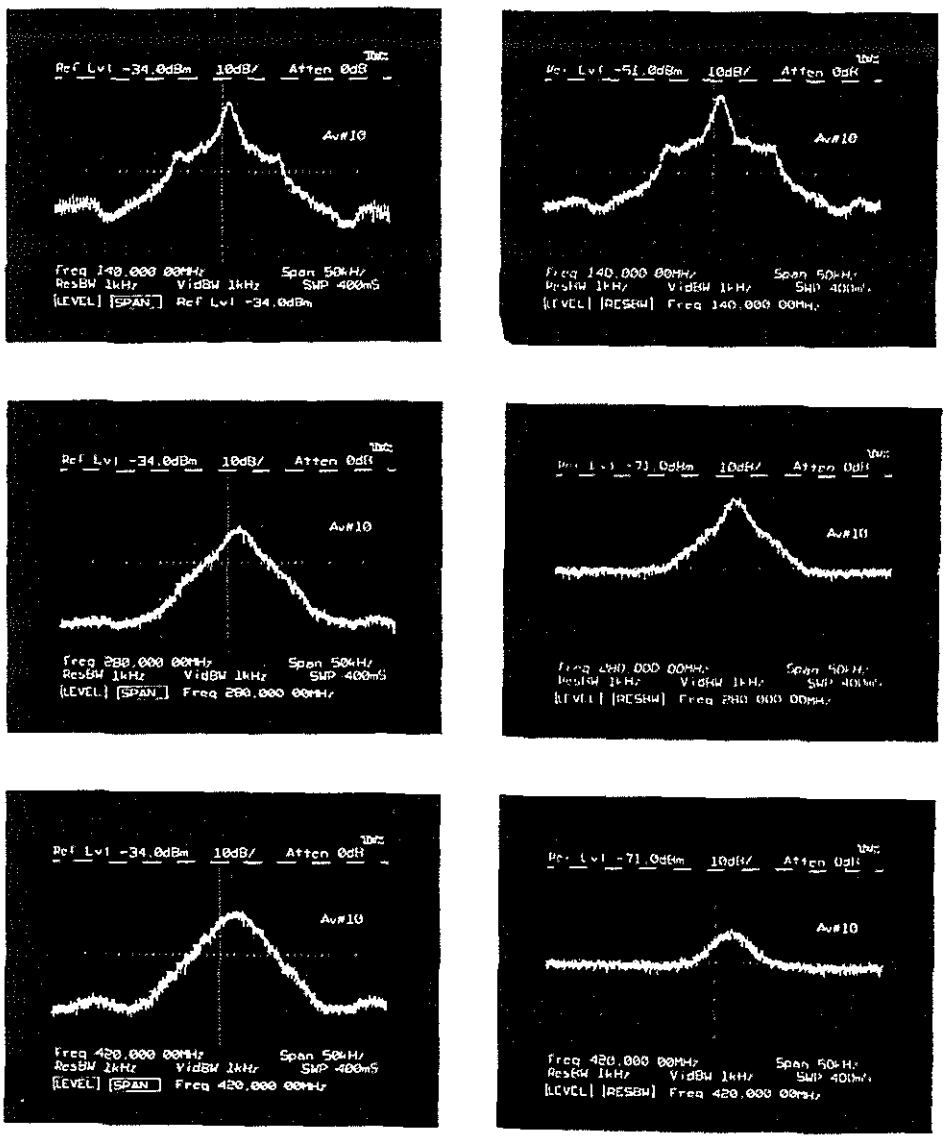

Figure 4.14: Beating spectrum of the RDSHI with and without EDFA compensation for the interferometer loss. With EDFA compensation, the S/N ratio does not decay as it does without the compensation.

4.2.3 Measurement

About 1 mW of output power from the EDFRL was coupled to the loss-compensated RDSHI. The linewidth of the EDFRL was measured between the wavelength of 1531 nm and 1538 nm, using the tenth order of the loss compensated RDSHI (corresponding resolution of 1.2 kHz). The beat spectrum (figure 4.15) was taken in the averaging mode of the spectrum analyzer (Tektronics model 2782) over several seconds with the resolution bandwidth setting at 1 kHz. The FWHM was calculated from the 3dB and 6dB point of these spectra assuming a Lorentzian lineshape. An upper bound on the natural linewidth was 2 kHz as given by the intersection of interferometer resolution and data plots in Figure 4.16. There was no noticeable dependence on the laser wavelength, laser power, RDSHI loss compensation, or co-dopant of the erbium fiber used in the EDFRL [15]. This suggests that another noise source is dominant over the natural linewidth of this laser. (The Schawlow-Townes linewidth, for example, has an inverse dependence on the laser power, and gives a sub-Hertz value for the EDFRL at these power levels [9].)

We concluded that the observed value is due to frequency jitter in the detected beatnote induced mainly by acoustic or thermal cavity length fluctuations of the EDFRL. To test this hypothesis requires a long delay line to give enough time for the laser to exhibit full root mean square (rms) frequency variation between the directly transmitted beam and the delayed beam. If the delay line is not long enough, then only a fraction of the full rms jitter will be measured. To do this, the beat spectrum was measured at every order (up to 30th) to determine the dependence of the FWHM

on the delay line length change (This is another advantage of the loss compensated RDSHI compared to the conventional method where the length of the delay is fixed [16]). The FWHM was again measured and calculated from the 3dB and 6dB point of the beat spectrum, assuming a Lorentzian lineshape. The mean FWHM of the beat spectrum saturated to a constant value of approximately 4 kHz after the 22nd order, and increasing deviation from the Lorentzian lineshape was evident (figure 4.16). To confirm that this broadening was from the laser, the experiment was repeated in three different cases, with acoustic isolation on the laser only, on the RSHDI only, and on both the laser and RSHDI. The result showed no detectable difference in FWHM of lineshape whether we provide an acoustic isolation on the RSHDI or not, but the acoustic isolation on the laser resulted in a narrower laser FWHM, indicating the main source of the laser frequency jitter is from cavity length fluctuations from the acoustic noise.

To conclude, the newly developed, improved RDSHI showed a peak resolution of 600 Hz with only 11 km of delay fiber (the resolution is wavelength dependent since the EDFA loss compensation has a dependence on the wavelength). The linewidth of the EDFRL has an upper bound less than 2 kHz, showing no dependence on the oscillation wavelength and output power of the laser. The measured frequency jitter was approximately 4 kHz. We attribute the frequency jitter to laser cavity length fluctuations from various perturbations such as thermal and acoustic noise. The time scale of these fluctuations is 1$\sim$2 msec.

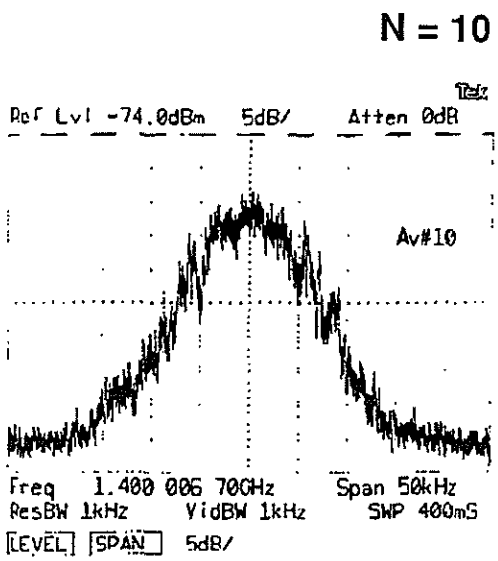

Figure 4.15: The beating spectra at 10th order under high resolution. By measuring 3dB and 6dB widths of the beating signal, the value of the linewidths at different orders were determined.

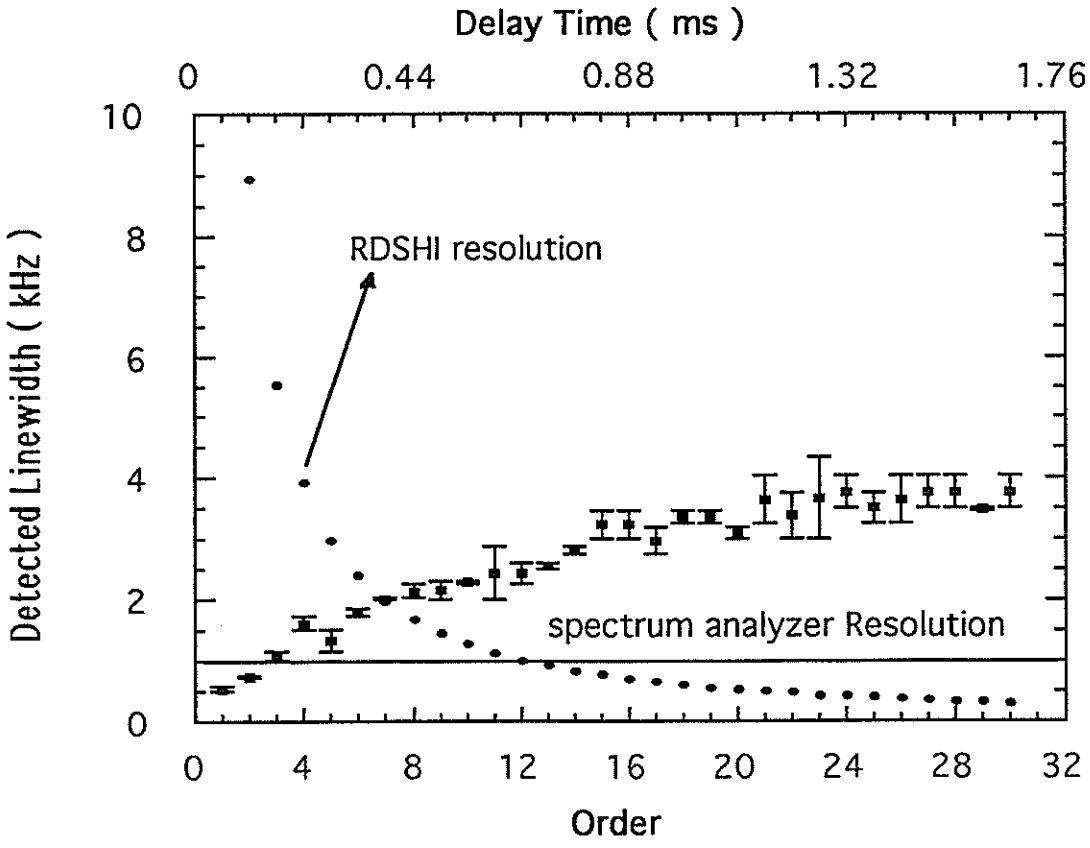

Figure 4.16: The measured linewidth dependence on the number of recirculations. The frequency jitter (upperbound for natural linewidth) saturates at 4kHz after 1.2ms.

Bibliography

[1] K. Vahala, and A. Yariv, IEEE J. Quantum Electron. **27**, 1096 (1983)

[2] R. M. shelby, M. D. Levenson, S. H. Perlmutter, R. G. DeVoe, and D. F. Walls, Phys. Rev. Lett., **57**, 691 (1986)

[3] S. Machida, and Y. Yamamoto, IEEE J. Quantum Electron., **22**, 617 (1986)

[4] S. Machida, Y. Yamamoto, and Y. Itaya, Phys. Rev. Lett., **58**, 1000 (1987)

[5] B. L. Schumaker, Opt. Lett., **5**, 189 (1984)

[6] H. P. Yuen, and V. W. S. Chan, Opt. Lett., **8**, 177 (1983)

[7] N. Park, S. Sanders, J. Dawson, and K. Vahala, Proc. Conf. Lasers and Electro-Otics, **CLEO 92**, (1992), paper CWE5

[8] S. Sanders, N. Park, J. Dawson, and K. Vahala, Appl. Phys. Lett., **61**, 1889, (1992)

[9] A. Yariv, Quantum Electronics, John Wiley and Sons, (1989)

[10] G. P. Agrawal, and N. K. Dutta, Long-wavelength Semiconductor Lasers, A Van Nostrand Reinhold Book, (1986)

[11] L. E. Richter, H. I. Mandelberg, M. S. Kruger, and P. A. McGrath, IEEE J. Quantum Electron., **22**, 2070 (1986)

[12] H. Tsuchida, Optics Letters **15**, 640 (1990)

[13] J. Dawson, N. Park, and K. Vahala, Photon. Tech. Lett., **4**, 1063 (1992)

[14] H. Okamura, and K. Iwatsuki, Electron. Lett., **26**, 1965 (1990)

[15] N. Park, J. Dawson, and K. Vahala, Opt. Lett., **17**, 1274, (1992)

[16] T. Okoshi, K. Kikuchi, and A. Nakayama, Electron. Lett., **16**, 630, (1980)

Chapter 5

Frequency Locking of an EDFRL to an External Cavity

Although quite stable, the EDFRL exhibits periodic mode hops on a time scale of minutes and experiences slow frequency drifts due to thermal and acoustic drift of the resonator. In this chapter an all-fiber stabilization scheme based on the Pound-Drever approach will be described, which eliminates mode hopping altogether and locks the lasing frequency to an external fiber Fabry-Perot resonator.

5.1 Pound-Drever method

There are numerous potential applications of stabilized laser sources, including WDM systems, fiber sensing networks, and spectroscopy. There have been several demonstrations to date of frequency stabilized lasers operating in the important 1.5μm telecommunications window. Techniques include absolute frequency stabilization us-

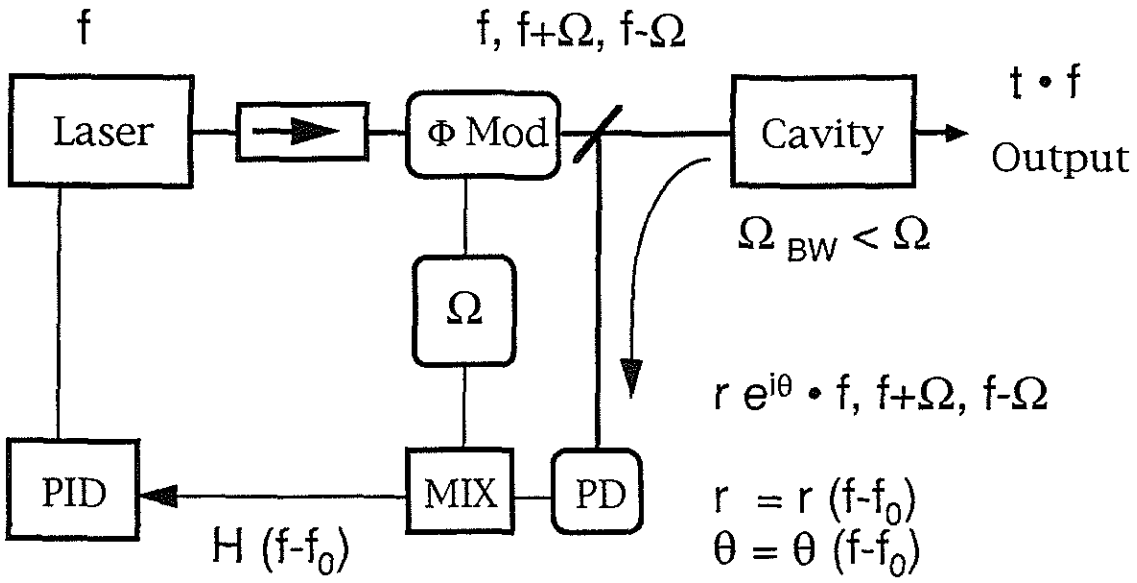

Figure 5.1: Illustration of the Pound-Drever technique which has been applied for locking an EDFRL to an external cavity.

ing atomic lines [1] and frequency locking to the resonance peak of a reference cavity using either the transmitted laser field [2] or the reflected laser field [3, 4]. For application to wavelength division multiplexed (WDM) systems, the Pound-Drever approach (i.e., reflected field method) is attractive since it provides evenly spaced multiple resonance peaks that can be shared by several lasers, and since the reflected wave approach provides response to laser phase fluctuations that is not limited by the reference resonator lifetime [3, 4].

Figure 5.1 shows a schematic diagram of the standard Pound-Drever technique. The output of the laser is phase modulated at frequency Ω which is bigger than the external reference Fabry-Perot filter bandwidth Ω_B. At this modulation frequency,

phase modulated sidebands are fully reflected from the filter, while the main carrier experiences partial reflection from the filter unless the laser frequency and the filter transmission peak match precisely. The fully reflected sidebands of the lasing field and the partially reflected lasing field are then coupled out through the bidirectional coupler and then photomix at the photodiode. Since the magnitude and phase of the reflected lasing field depends on the frequency deviation of the reflected field (f_{Laser}) relative to the transmission peak of the FFP cavity (f_{FFP}), the demodulated photomix signal at the mixer output gives the sign and magnitude of the deviation [3]. Frequency tracking is then attained by processing this error signal through RF bandpass filters and a proportional integral differential (PID) control circuit, and feeding the correction signal back to the laser.

If the laser and the reference filter match in frequency precisely as a result of frequency tracking, but if the laser phase still fluctuates with a speed faster than the decay time of the reference cavity, the direct reflection from the input mirror cannot have perfect antiphase relation with the leakage field from the field stored in the reference cavity. When added together, this results as a partial reflection of the main carrier from the cavity. This partially reflected main carrier then generates the beating signal at the photodetector with the reflected sidebands, which can be processed in a similar way as in the case of frequency tracking to get feedback signal for the phase change. In this way the Pound-Drever approach gives control over the phase of the laser as well as frequency.

5.2 Implementation of the locking technique to the fiber laser

Figure 5.2 shows the implementation of Pound-Drever technique to fiber laser, which was extended and further developed to achieve both the laser stabilization and frequency locking at the same time. Added components in the fiber laser include a phase modulator and a metal clad fiber for laser cavity length control. The stabilization system consists of two independent control circuits. The first causes the internal mode selection FFP filter to track the lasing frequency as it drifts or shifts due to tracking provided by the second control circuit. This first circuit eliminates mode hopping. The second circuit causes the lasing frequency to track a particular resonance of the external fiber FFP reference. Both circuits utilize the Pound-Drever method. For the first circuit, the frequency deviation error signal between the lasing mode and the internal mode selection FFP filter was obtained by placing an electro-optic phase modulator inside the ring, immediately before the output coupler and internal mode selection FFP filter as illustrated. The phase modulator was driven at 300 MHz. At this frequency the phase modulation sidebands were well outside the FFP bandwidth of 50 MHz insuring nearly full reflection of the sidebands. Full reflection also prevents any possibility of unintentional mode-locking by the phase modulator. The fully reflected sidebands of the lasing field and the partially reflected lasing field are coupled out of the ring using the bidirectional coupler as illustrated and then photomix at the photodiode (D1). The demodulated photomix signal at the mixer output gives the sign and magnitude of the deviation [3]. Frequency tracking is then attained by

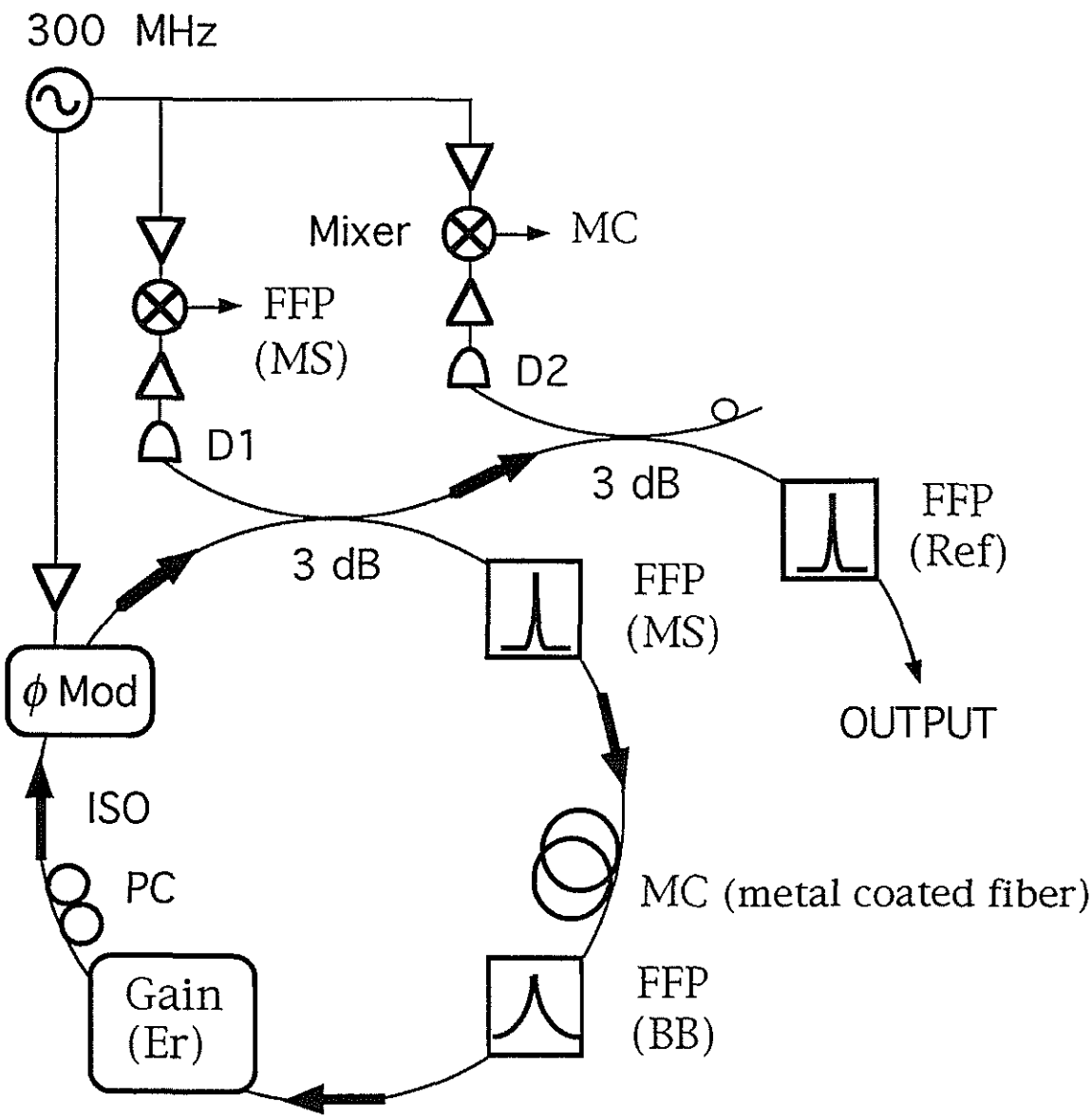

Figure 5.2: This picture shows the feedback diagram for the EDFRL. By placing the phase modulator inside the cavity, it was possible to get the error signal for locking and stabilization at the same time. The error signal between the laser and the narrow bandpass filter was fed back to the filter inside the cavity, and the error signal between the laser and the reference fiber Fabry-Perot filter was fed back to the metal clad fiber to adjust the cavity length of the laser.

processing this error signal through a RF bandpass filter (BW 30MHz), RF amplifier (50dB) and a PID control circuit (BW 10kHz), and feeding it back to the controlling voltage of the mode-selection FFP filter. Figure 5.3a shows the error signal obtained with and without the feedback loop in operation. Without the feedback (lower curve), the acoustically unshielded laser gives frequent mode hops, resulting in an error signal of about 10MHz (corresponding to 3~4 longitudinal modes). Once feedback is engaged, a significant reduction of the error signal is apparent. The resulting mode-hop-free operation of the laser was confirmed by monitoring the lasing spectrum using a Super-Cavity scanning interferometer. Without any acoustical shielding of the laser and with the introduction of intentional acoustic disturbances, no mode hops were observed over periods of several hours.

To lock the laser frequency to the external FFP cavity, an additional 3dB fiber coupler and the reference FFP cavity (closely matched with the internal mode selection FFP) were added after the output port of the ring laser as illustrated. Even though the laser output was modulated at 300MHz, after the external 50MHz bandwidth FFP, the sideband at 300MHz was 20dB smaller than the main carrier. The partly reflected field from the reference FFP cavity was detected at photodiode 2 (D2), processed in the same way as described for the first servo loop, and then converted to a current used to resistively heat a metal clad fiber (MCF, 1.5 meter long, 2 ohm resistance) making up part of the laser ring. This has the effect of controlling the overall laser ring optical path length. The tuning range achievable by resistive heating alone was approximately 200 MHz with a corresponding maximum current

of 500 mA. This range and the MCF response time of 4 millisecond were sufficient to compensate the relative drift of the external reference FFP cavity and laser frequency due to thermal variations. Once locked, it was possible to observe laser wavelength tracking of the transmission peak of the external reference FFP cavity, either by observing the optical spectrum using the Super-Cavity scanning interferometer or by monitoring the applied voltage on the mode selection FFP filter inside the cavity. Within the limited tracking range of 200 MHz, due to the limited applied current on the MCF, the laser wavelength varied linearly with the external FFP tuning voltage. Figure 5.3b shows the error signal obtained from the external FFP cavity servo loop with and without the feedback loop engaged. Error signal reduction is again apparent for the case of the engaged loop.

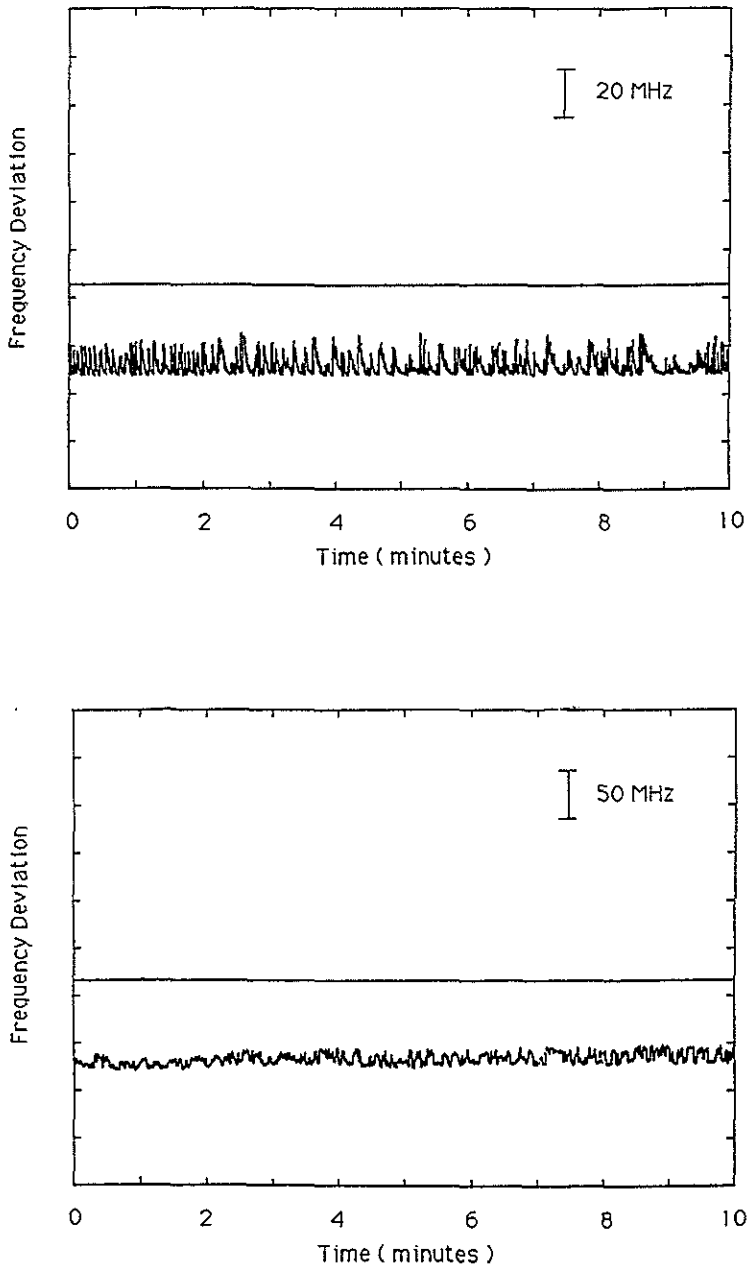

Figure 5.3: The picture shows the error signal from the feedback circuitry with and without the feedback circuit engagement. The upper graph shows the error between the laser and mode selection filter, and the bottom graph shows the frequency deviation between the laser and reference cavity.

Bibliography

[1] Y. C. Chung, R. M. Derosier, H. M. Presby, C. A. Burrus, Y. Akai, and N. Masuda, Photon. Technol. Lett., **3**, 841 (1991)

[2] W. Vassen, C. Zimmermann, R. Kallenbach, and T. W. Hansch, Optics Comm., **75**, 435 (1990)

[3] R. W. P. Drever, J. L. Hall, F. V. Kowalski, J. Hough, G. M. Ford, A. J. Munley, and H. Ward, Appl. Phys. B **31**, 97 (1983)

[4] T. Day, E. K. Gustafson, and R. L. Byer, IEEE J. Quantum Electron., **28**, 1106 (1992)

Chapter 6

Application of EDFRL to Four-Wave Mixing

By investigating the response function of the semiconductor optical amplifier under high frequency optical modulation, it is possible to obtain useful information about the amplifier dynamics at high speed. As a pump laser for this purpose, the EDFRL is most advantageous due to its ultranarrow linewidth, quantum limited intensity noise, and wide tuning range. In this chapter, THz optical modulation dynamics inside the semiconductor optical amplifier will be studied and interpreted as a highly nondegenerate four wave mixing process inside a nonlinear optical medium. Attemps will be made to analyze the FWM process with wavelength conversion applications in mind.

6.1 FWM in the traveling wave amplifier

A semiconductor optical amplifier (SOA, or traveling wave amplifier, TWA) is a traveling wave device for the optical amplification of the signal. In its simplest form, it is an anti-reflection coated semiconductor laser. Even though the semiconductor TWA has advantages over EDFA in terms of compactness and compatibility for integrated optics, the gain competition in multichannel operation severely limits the application of this device as an optical amplifier. Still, there exist many other applications for the TWA, such as an optical switch or a wavelength converter [2, 3]. For applications like these in the high data rate regime, it is critical to understand the ultrafast dynamics of the semiconductor TWA to find proper design considerations and performance limitations.

These ultrafast dynamics inside the TWA include both interband and intraband mechanisms. Intraband dynamics includes several different mechanisms, such as carrier heating, carrier cooling, and spectral hole burning [4, 5]. Figure 6.1 illustrates the effect of carrier heating and spectral hole burning on the TWA gain spectrum.

Compared to the speed of the interband process (~200ps), intraband processes are very fast (< ps), and require special techniques to characterize. Traditionally, to study these ultrafast mechanisms, ultrashort (< 100fs) optical pulses are used to excite and probe the response of the system [5]. This approach, even though physically clear and direct, has difficulties in achieving a temporal resolution better than 80fs, because of the pulse broadening inside the TWA, which results from the self phase modulation induced by the large peak power [4].

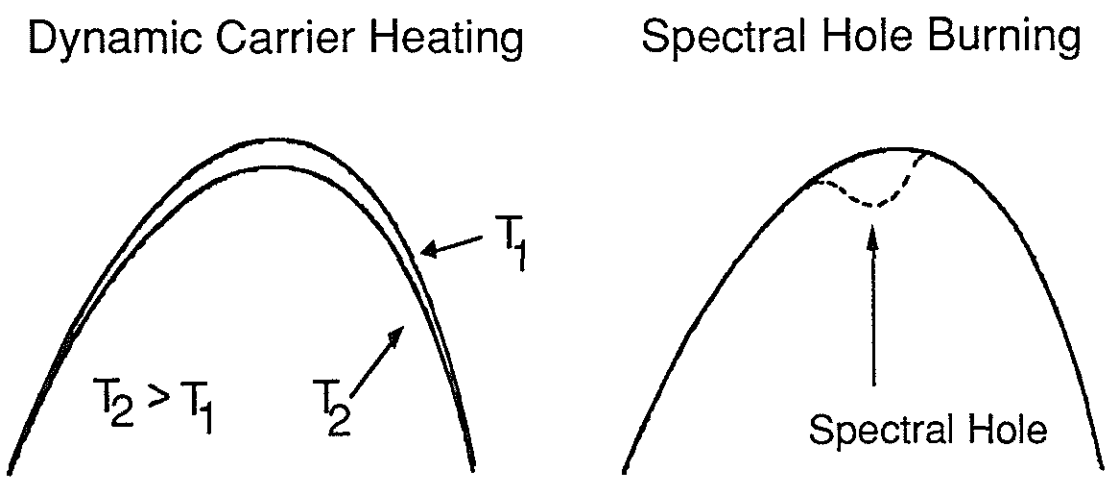

Figure 6.1: Intraband dynamics involved with the nonlinear gain dynamics in TWA. The carrier heating is related to electron temperature dissipation to the lattice, and the spectral hole burning is related to the electron-electron interaction, through which neighboring electrons fills holes in the electron energy distribution.

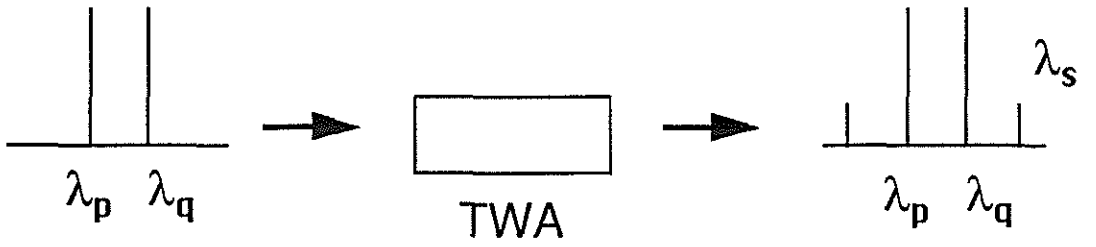

Figure 6.2: Schematic diagram for the FWM process in the TWA. The beating signal generates dynamic grating inside the TWA which forward scatters the input beam, while shifting the frequencies of the beams with the amount of beating frequency.

Another approach uses the four-wave mixing process [6]. By mixing two waves at different frequencies within the TWA, a grating can be generated in the gain and the index of the TWA. This dynamic grating then forward scatters and frequency shifts the injected beams to make sidebands. Since the formation and dissipation of these grating is a function of modulation dynamics, it is possible to determine the strength and the time constant of associated dynamics from the size of the generated sidebands.

Picture 6.2 shows the schematic diagram for the FWM process in the TWA. For injected beams $E_{p,q}$ (p=pump, q=probe), the evolution of sidebands ($E_s^{+,-}$) follows formulae [3]

$$\frac{dE_{p,q}(z)}{dz} = \frac{1}{2}\left(\frac{g_0}{1+\frac{P(z)}{P_s}}(1-i\alpha)-\alpha_l\right)E_{p,q}(z) \tag{6.1}$$

$$\frac{dE_s(z)}{dz} = \frac{1}{2}\left(\frac{g_0}{1+\frac{P(z)}{P_s}}(1-i\alpha)-\alpha_l\right)E_s(z) \tag{6.2}$$
$$-\kappa(z)E_p^2(z)E_q^*(z)\ exp\ (i\Delta kz)$$

where $\Delta k = 2k_p - k_q - k_s$ is the phase mismatch between the beams due to the dispersion in the TWA, and

$$\kappa(z) = \frac{1}{2}\frac{g_0}{1+\frac{P(z)}{P_s}}\sum_{m=1}^{3}\frac{1-i\alpha_m}{1-i2\pi f\tau_m}\cdot\frac{1}{P_m} \tag{6.3}$$

is the coupling parameter for the FWM process. Also α_l is the waveguide loss, g_0 is the small signal gain, P_m is the saturation power for different nonlinear gain processes, α_m is corresponding alpha parameter, and τ_m is the time constant of the processes.

When solved, it is possible to get an expression for E_s in terms of $E_{p,q}$ at the end of the TWA.

$$E_s(l) = -\frac{E_p^2(l)E_q^*(l)\kappa(l)le^{i\Delta kl}}{0.23G+i\Delta kl} \tag{6.4}$$

$$= E_p^2(l)E_q^*(l)\sum_{m=1}^{3}\frac{c_m}{1-i2\pi f\tau_m} \tag{6.5}$$

where

$$G = 4.34\int_0^l(\frac{g_0}{1+\frac{P(z)}{P_s}}-\alpha_l)dz \tag{6.6}$$

is the gain of the TWA (in dB). By using equation 6.5 and experimental data, it is possible to estimate the time constant (τ_m) and strength (c_m) of related dynamics [11].

6.2 Application of EDFRL to the FWM experiment

As the modulation frequency increases, the size of the sideband decays rapidly (~20dB per decade), and it is often hard to directly detect the sideband using an optical spectrum analyzer. This problem can be overcome by using optical heterodyne detection

with a narrow linewidth source, such as a fiber laser. Compared to the usual linewidth of semiconductor lasers (> 1MHz), the much narrower linewidth of fiber lasers (< 4kHz) [10] produce narrower linewidth sidebands when the lasers were used as pump sources in the FWM process. Again when combined with the narrow linewidth fiber laser local oscillator, the detected signal at the spectrum anayzer (with narrow resolution bandwidth setting) produces a much higher signal to noise ratio than the direct detection system [6, 11]. The quantum limited intensity noise [8, 9], frequency stability and broad tuning range [7] of the laser also contribute to get a clear spectrum.

Figure 6.3 shows the experimental setup used for the measurement. Outputs of two tunable fiber lasers ($f_{p,q}$) were mixed using a 3dB fused fiber coupler. By using a polarizer and polarization controllers, these beams were polarization matched and then coupled to the TWA to generate the beating. The optical power coupled to the TWA was about 250μW. The TWA used in the experiment was a tensile strained InGaAs/InGaAsP multiple quantum well device operating at 1.5μm [12]. The optical gain was estimated to be about 17dB with gain ripple as low as 0.1dB. Optical isolators were placed at each end of the TWA to suppress the optical feedback from the fiber cleaves.

The generated signal (sideband) at $2f_p - f_q$ was heterodyne-detected by using a third fiber laser as a local oscillator. The magnitudes of the beating signals were measured from a microwave spectrum analyzer at a fixed frequency of 4.0GHz (resolution bandwidth set at 30kHz), to eliminate frequency dependence of the detector (corner frequency 16GHz) and the microwave amplifier (40dB, $2 \sim 8$GHz). The FWM

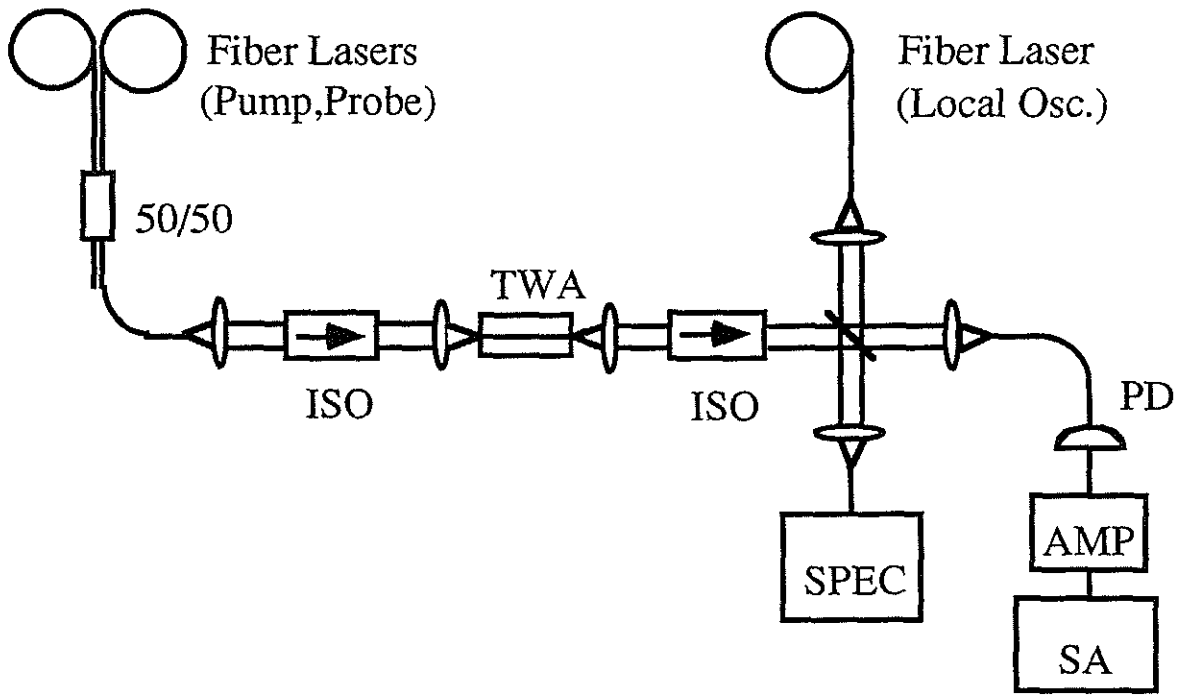

Figure 6.3: Measurement setup for the FWM experiment. Two fiber lasers were used to generate the beating signal, which generates sidebands through the FWM process in the TWA. A third fiber laser was used as a local oscillator for the sideband detection.

signals were measured for detuning frequencies from -1.7THz to 1.5THz. Due to the quantum limited intensity noise and narrow linewidth of the fiber laser, and the noise rejection from the narrow resolution bandwidth in spectrum analyzer, the sensitivity of the detection system was very high, and the signal to noise ratio was still as high as 20dB at the maximum detuning frequency [11]. The detuning frequency was mainly limited by the tuning capability of one of the lasers arising from the restricted FSR of tunable FFP.

Figure 6.4 shows the normalized signal power (circles) as a function of detuning frequency featuring excellent fit with the theoretical model (equation 6.5). One set of parameters was used for both negative and positive detuning frequencies, with the following values; $c_1 = 5.65e^{-i1.30}$ and $\tau_1 = 200ps$ for the interband transition, $c_2 = 0.0642e^{i1.30}$ and $\tau_2 = 650fs$ for the dynamic carrier heating, and $c_3 = 0.0113e^{i1.53}$ with $\tau_3 = 50fs$. Since the temporal resolution of this experiment was limited to 94fs ($\tau = 1/2\pi\Delta f$), it was not possible to exactly determine the dynamics involved with τ_3. Improved tuning range and temporal resolution should be able to resolve the dominant contributing mechanism below the 100fs regime.

6.3 Wavelength Conversion with FWM

One of the possible applications of the four-wave mixing process is wavelength conversion of optical beams for the WDM system. Wavelength conversion can be achieved by injecting a signal beam at frequency f_q along with a pump source at f_p to the nonlinear medium. The four-wave mixing process then generates the wavelength shifted,

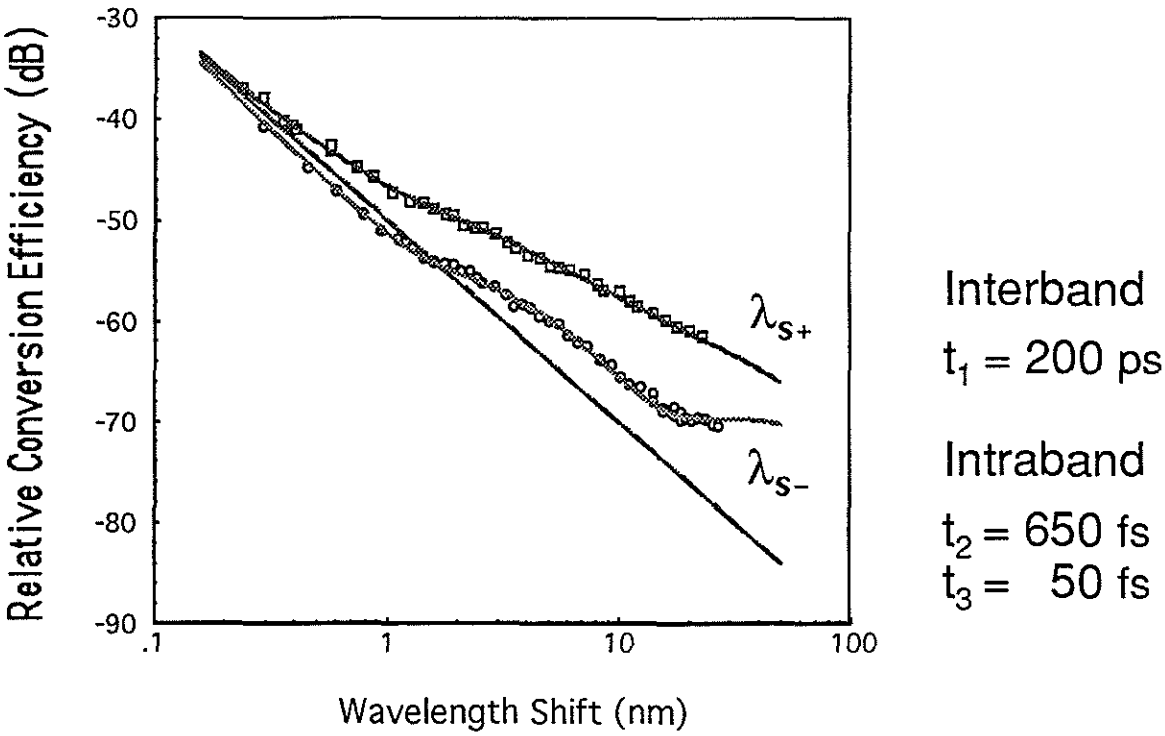

Figure 6.4: Data shows the measured sideband strength as a function of detuning frequencies. The solid line is a fitting curve with 3 different mechanisms. A single set of parameters was used both for the positive and negative side of the sidebands. The used value for t_3 is below the resolution limit of this experiment, and can have any value below 90fs.

phase conjugate image (E_s) of signal beam (E_q) at $2f_p - f_q$ (figure 6.2). Although the conversion efficiency of this process is not high with ordinary nonlinear media, it is possible to get sufficient signal levels when it is combined with an optical amplifier. This idea has been implemented both with a TWA [2] and a dispersion shifted fiber (DSF) [13] as the conversion medium. Even though DSF provides a much lower noise penalty on the wavelength shifted signal due to the passive nature of the fiber FWM process, the wavelength conversion range is much too limited because of the weak nonlinearity of fiber, which dictates the use of a long length of fiber and thus accumulation of group velocity dispersion. As a result, the FWM process in fiber lacks with the tunability since the pump wavelength must be matched at the zero dispersion wavelength of the fiber.

In contrast, a TWA has a relatively high nonlinear coefficient, and the dispersion problem can be avoided [3]. The conversion efficiency of the TWA FWM process can be derived from the equation 6.5. When expressed in terms of dB, the efficiency η can be written as,

$$\eta = 10\log\frac{P_s(l)}{P_q(0)} = 3G + 2I_p + 20\log\left|\sum_{m=1}^{3} c_m \cdot \frac{1}{1 - i2\pi f\tau_m}\right| \qquad (6.7)$$

Noting that c_m and τ_m are related with the intrinsic dynamics which cannot be adjusted, the easiest way to increase the conversion efficiency is either to increase the gain of TWA (G) or to increase the input pump power (I). Based on this concept, it is possible to estimate the gain necessary to achieve lossless conversion ($\eta = 0$) from equation 6.7. The theoretical plot to achieve lossless conversion (figure 6.5) shows the gain values in feasible range with existing technology.

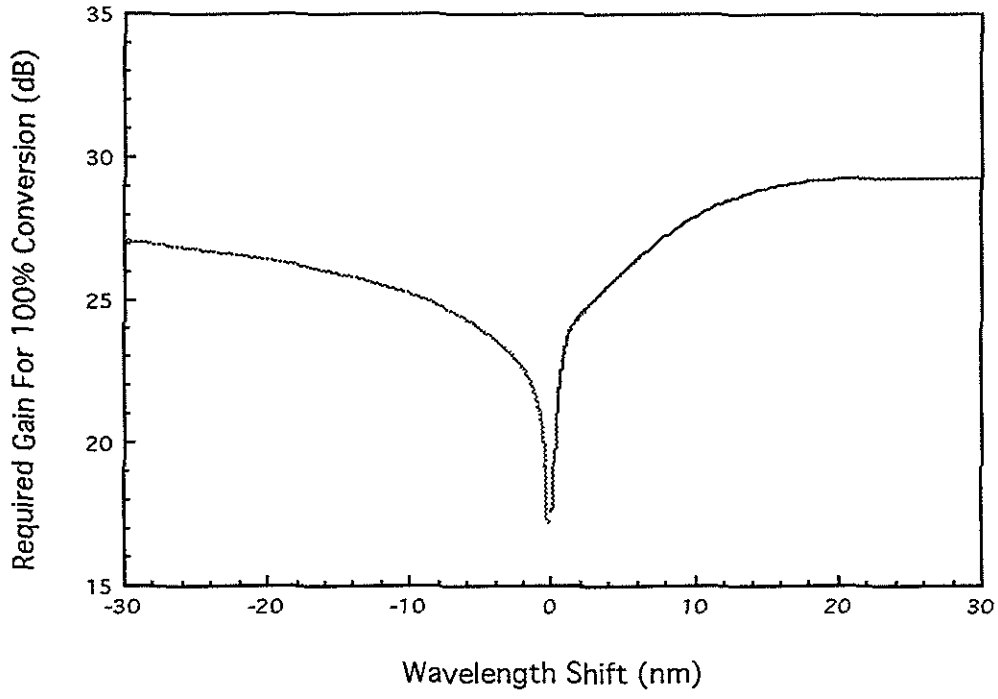

Figure 6.5: The estimated gain (saturated) to achieve lossless conversion at 0.1mW input pump power

Bibliography

[1] T. L. Koch, and U. Koren, IEEE J. Quantum Electron., **27**, 641 (1991)

[2] K. Inoue, Electron. Lett, **23**, 911 (1987)

[3] J. Zhou, N. Park, J. Dawson, K. Vahala, M. Newkirk, and B. Miller, Photon. Tech. Lett., **6**, 50, (1994)

[4] K. L. Hall, G. Lenz, E. P. Ippen, U. Koren, and G. Raybon, Appl. Phys. Lett., **61**, 2512, (1992)

[5] K. L. Hall, J. Mark, E. P. Ippen, and G. Eisenstein, Appl. Phys. Lett., **56**, 1740, (1990)

[6] K. Kikuchi, M. Kakui, C. E. Zah, and T. P. Lee, IEEE J. Quantum Electron., **28**, 151 (1992)

[7] N. Park, J. Dawson, K. Vahala and C. Miller, Appl. Phys. Lett., **59**, 2369, (1991)

[8] N. Park, S. Sanders, J. Dawson, and K. Vahala, Proc. Conf. Lasers and Electro-Otics, **CLEO 92**, (1992), paper CWE5

[9] S. Sanders, N. Park, J. Dawson, and K. Vahala, Appl. Phys. Lett., **61**, 1889, (1992)

[10] N. Park, J. Dawson, and K. Vahala, Opt. Lett., **17**, 1274, (1992)

[11] J. Zhou, N. Park, J. Dawson, K. Vahala, M. Newkirk, and B. Miller, Appl. Phys. Lett., **63**, 1179, (1993)

[12] B. I. Miller, U. Koren, M. A. Newkirk, M. G. Young, R. M. Jopson, R. M. Derosier, and M. D. Chien, Photon. Tech. Lett., **5**, 520, (1993)

[13] K. Inoue, T. Hasegawa, K. Oda, and H. Toba, Electron. Lett., **29**, 1708, (1993)

Appendix A

Mode Locked Operation of Fiber Lasers

One of the important application of the EDFA is to the mode locked fiber laser for ultrashort pulse generation. This appendix will describe the principles and construction of a passively mode locked fiber laser, along with brief discussions about fiber nonlinearity and soliton propagation inside the fiber.

A.1 Nonlinearities in fiber

With EDFAs in the system, it is possible to increase the available span length of fiber in all-optical, electrically-passive manner. This leads to new kinds of system problems. Compared to regenerator based systems, where the correction for the optically induced noise is possible at every amplification stage (with electrical filters and clock recovery circuits), the EDFA based systems cannot remove the nonlinearity,

and ASE induced noise at the amplification stage. Noise therefore accumulates as the span length increases. The increasing data bit rate also provides more favorable conditions for the nonlinear dynamics related noise to participate, because the peak power for each bit pulse needs to be increased to keep the total number of photons per bit at the same number. The reduced core size of a dispersion shifted fiber also makes it easier for nonlinear dynamics in fiber to play a part.

Nonlinearities include stimulated Brioullin scattering (SBS), stimulated Raman scattering (SRS), and self phase modulation (SPM) [1]. In WDM system, four-wave mixing in the dispersion shifted fiber also can add errors to the signal [1]. Group velocity dispersion (GVD) in fiber also can work with the nonlinearities, to make the noise dynamics more complex. Suppressing these mechanisms is thus of importance in improving the system performance. Of these mechanisms, dispersion or SPM is especially difficult to remove compared to other noise sources, due to their inherent presence in the material itself.

A totally different approach to this problem starts from an equation (nonlinear Schroedinger equation : NLSE) which inherently accommodates dispersion and self phase modulation effect [1]. In its simplest form, the nonlinear Schroedinger equation can be written as;

$$i\frac{\partial A}{\partial z} = \frac{1}{2}\beta_2\frac{\partial^2}{\partial T^2}A - \gamma \mid A \mid^2 A - i\frac{\alpha}{2}A \quad (\alpha = 0 : NLSE) \qquad (A.1)$$

where A is the optical field strength, β_2 is a dispersion term, γ is a nonlinear index parameter, and α is a loss factor of the fiber. When normalized using the parameters,

$$u = \left[\frac{\gamma T_0^2}{\mid \beta_2 \mid}\right]^{\frac{1}{2}} A \quad , \quad \tau = T/T_0 \quad , \quad \xi = z \mid \beta_2 \mid /T_0^2$$

the equation can be expressed in terms of unitless parameters

$$i\frac{\partial u}{\partial \xi} = sgn(\beta_2)\frac{1}{2}\frac{\partial^2}{\partial \tau^2}u - |u|^2 u \tag{A.2}$$

(Here T_0 is the pulse width, u is the normalized optical field, and ξ is the normalized fiber length. For a reference, the typical value of these parameters are : $\beta = -20ps^2/km$, $\gamma = 20W^{-1}km^{-1}$, $T^0 = 1ps$.) with the following solution.

$$u(\xi,\tau) = Nsech(\tau)exp(i\xi/2) \tag{A.3}$$

(N is usually referred as the soliton number, and is involved with higher order soliton behavior, such as soliton pulse compression). Any pulse which satisfies the solution A.3 thus can retain its shape as it propagates through the nonlinear, dispersive medium.

Figure A.1 illustrates the numerically simulated propagation of a soliton and a square pulse under the influence of SPM and dispersion, using standard method of split-step and FFT [2]. The resistance of the soliton against SPM and dispersion is again evident. Thus soliton based communication system can achieve lower bit error penalty than for the case of modulated CW laser.

A.2 Mode locked fiber laser

Generation of solitons has been demonstrated in several different ways. Most of these methods are based on the self-adjusting character of the soliton. For example, by amplifying a mode-locked pulse from a semiconductor laser, it is possible to achieve critical pulse power to induce enough nonlinearity and adjust the shape of the pulse

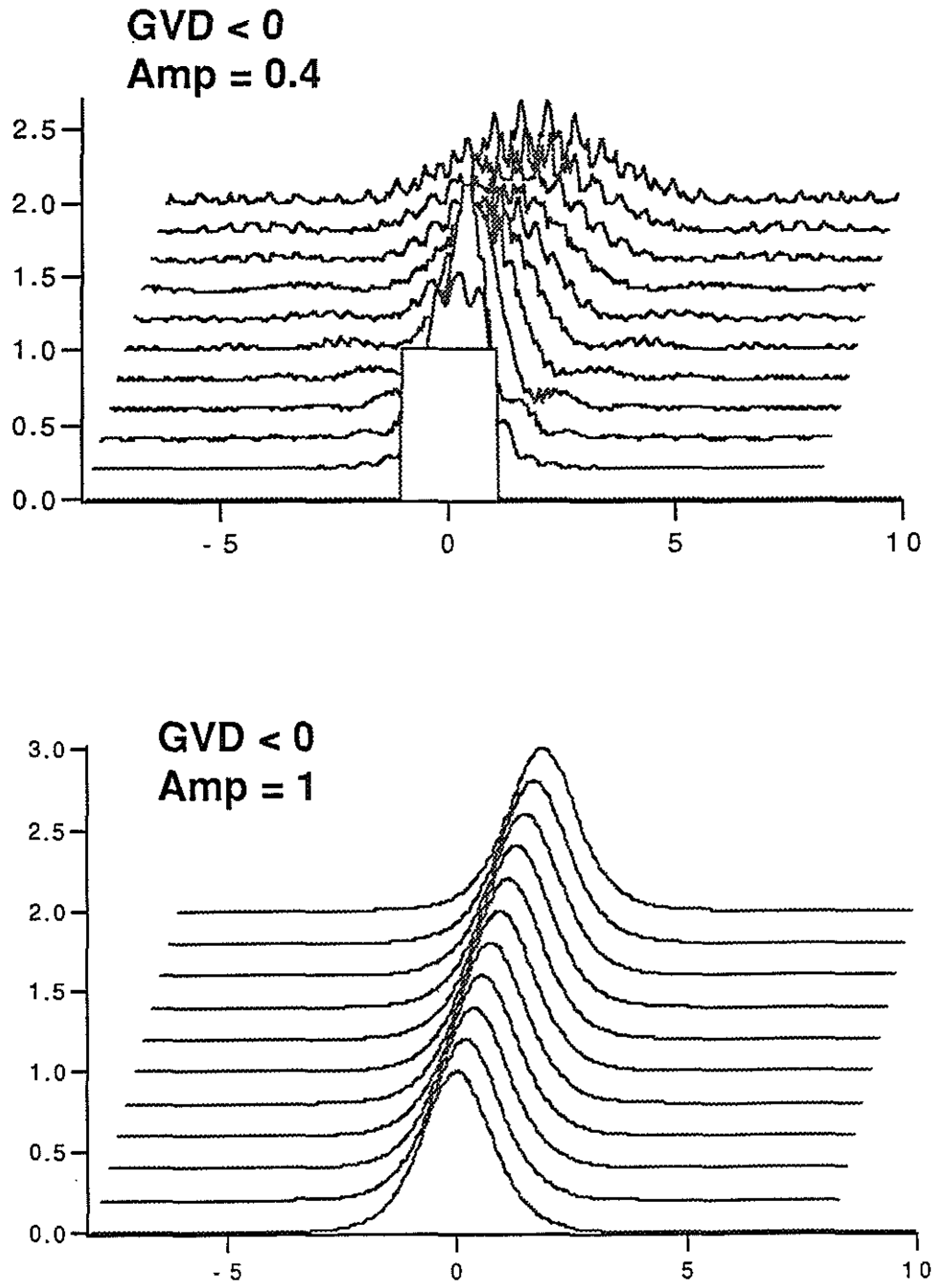

Figure A.1: The pulse breakup of a square pulse under the influence of dispersion and nonlinearity. For comparison, the soliton keeps the shape of the pulse as it propagates through the same medium, even with higher peak power.

towards a soliton.

Recent approaches include the generation of solitons from the fiber laser. Since the laser cavity of fiber laser itself satisfies the nonlinear Schroedinger equation, the pulse output from the cavity would have more tendency to be a soliton. The chirping behavior which is common to the mode locked SDL-amplifier scheme does not appear in this case neither. For example, by using the passively mode locked figure 8 laser, with a short segment of fiber at the end of the output for soliton pulse compression, it is possible to generate 30fs pulses at hundreds of MHz repetition rate [3]. For higher bit rate pulses, higher-order active mode locking can be applied to generate 20Gb/s rate picosecond pulses [4, 5].

Figure A.2 shows the structure for the one of the possible configuration of passively mode locked fiber lasers. The inset shows a nonlinear optical loop mirror, which acts as a saturable absorber in this case [6]. Briefly, the 3dB coupler splits the signal into two different paths, one of which goes through the amplification process first and then propagates (counter clockwise), and another one which goes through the loop first and the amplifier later (clockwise). Even though the amplified signals have the same intensity as they exit the loop, they have different phase due to the accumulated nonlinear index difference ($n = n_0 + n_2 I$, and $I = GI$ *or* I, depending on the path taken). The transmission function of the NALM ($T = \frac{G}{2}\left[1 + Cos\left(\frac{\pi n_2 (1-G)|E_{IN}|^2 L}{\lambda}\right)\right]$) resulting from this phase interference thus amplifies appropriate pulses with high power while suppressing weak sidebands. Figure A.4 shows the pulse train at a repetition rate of 125kHz, from the constructed figure 8 laser. The output of the

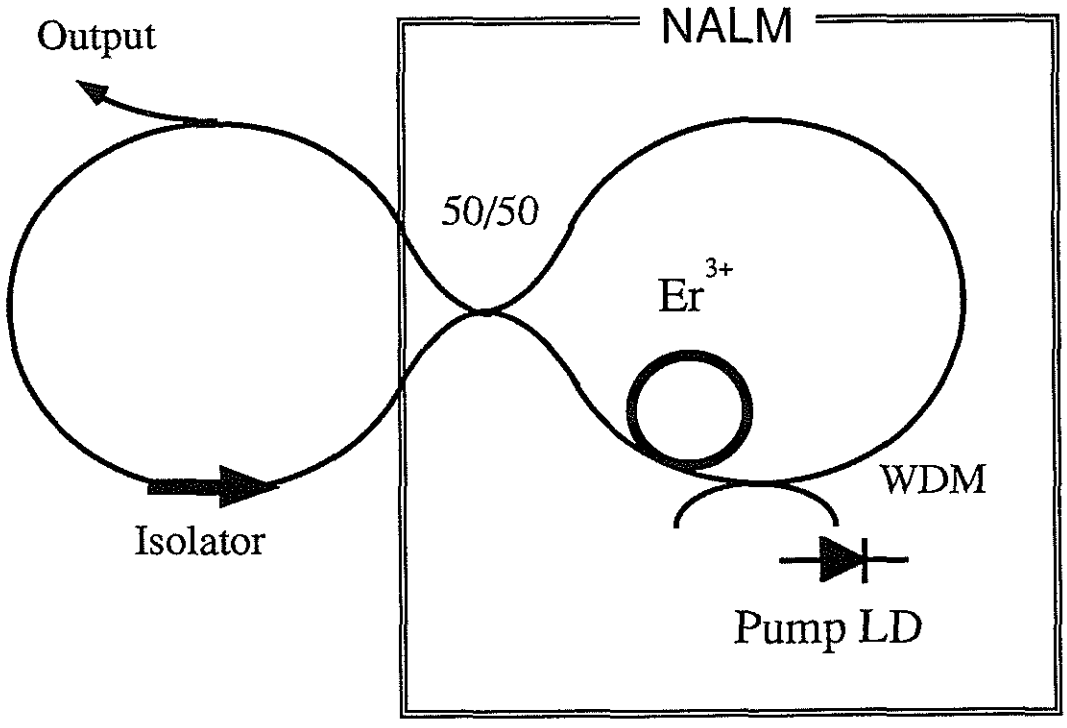

Figure A.2: Schematic diagram of the passively mode-locked figure 8 laser. The inset acts as a saturabable absorber for mode locked operation.

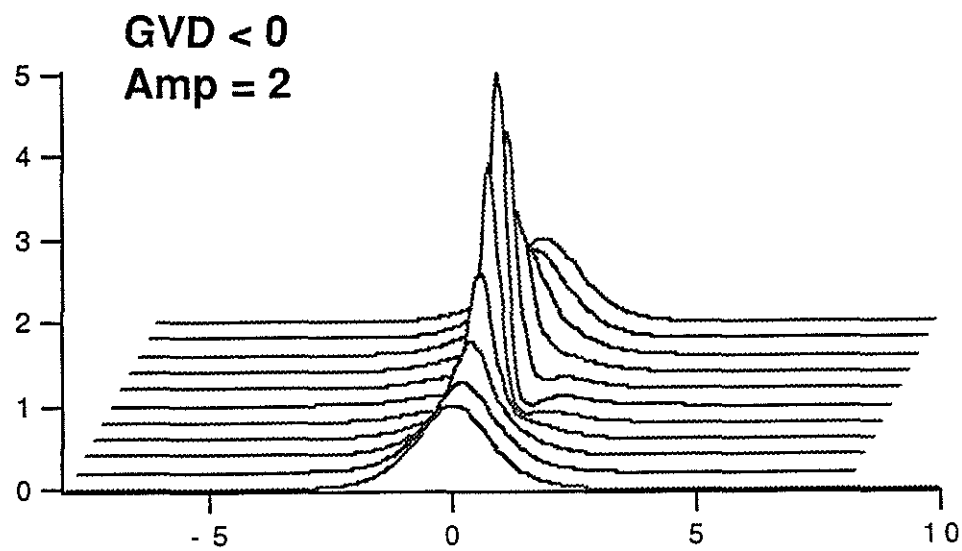

Figure A.3: This picture shows how an output pulse from a mode locked fiber laser can be further compressed. By appropriately amplifying the output of the laser, and letting the pulse evolve over the adjusted length of a fiber, it is possible to further compress the width of pulse in time domain.

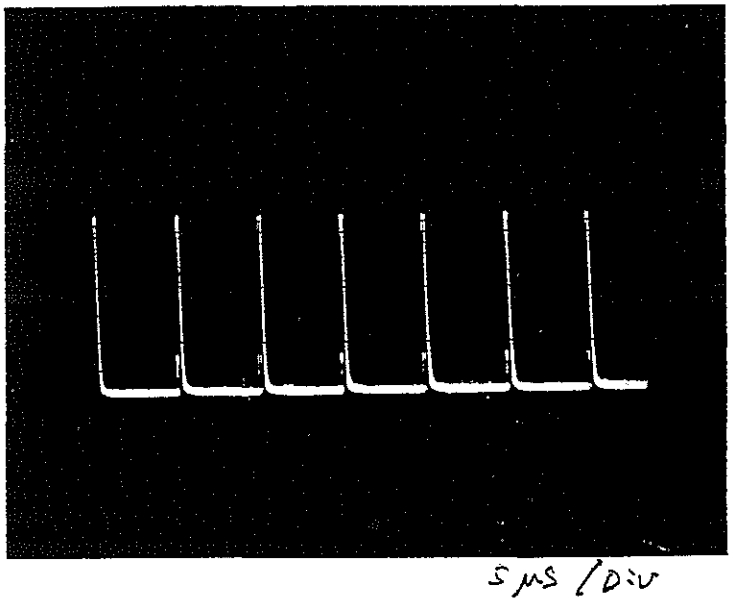

Figure A.4: This picture shows the output of a mode locked laser at a repetition rate of 125kHz.

laser also can be further amplified to satisfy conditions for a higher order soliton and then can be compressed by adding the right length of fiber at the output port of the laser (figure A.3). The application of the passively mode locked laser is limited to spectroscopic usages due to the low repetition rate. For communications applications, it is desirable to add a modulator (usually in a ring configuration) inside a cavity to achieve a much higher repetition rate.

Bibliography

[1] G. P. Agrawal, Nonlinear fiber optics, Academic Press (1989)

[2] W. H. Press, B. P. Flannery, S. A. Teukolsky, and W. T. Vetterling, Numerical recipes in Pascal, Cambridge University Press (1989)

[3] D. J. Richardson, A. B. Grudinin, and D. N. Payne, Electron. Lett. **28**, 778 (1992)

[4] H. Takara, S. Kawanishi, and M. Saruwatari, Electron. Lett. **29**, 1149 (1993)

[5] A. D. Ellis, T. Widdowson, X. Shan, G. E. Wickens, and D. M. Spirit, Electron. Lett. **29**, 990 (1993)

[6] A. P. O'neill, and R. P. Webb, Electron. Lett., **24**, 2009 (1990)